

Dissociative Chemisorption of Methane on Ni and Pt Surfaces: Mode-Specific Chemistry and the Effects of Lattice Motion

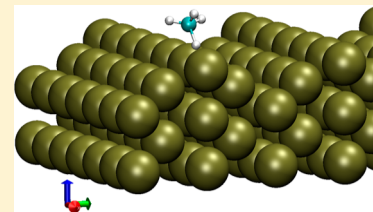
Sven Nave,[†] Ashwani K. Tiwari,[‡] and Bret Jackson^{*,§}

[†]Institut des Sciences Moléculaires d'Orsay, Université Paris-Sud 11/CNRS-UMR 8214, Université Paris-Sud, Bât. 351, 91405 Orsay Cedex, France

[‡]Indian Institute of Science Education and Research Kolkata, Mohanpur 741252, India

^{*}Department of Chemistry, University of Massachusetts, Amherst, Massachusetts 01003, United States

ABSTRACT: The dissociative chemisorption of methane on metal surfaces is of great practical and fundamental interest. Not only is it the rate-limiting step in the steam reforming of natural gas, but also the reaction exhibits interesting mode-specific behavior and a strong dependence on the temperature of the metal. Electronic structure methods are used to explore this reaction on various Ni and Pt surfaces, with a focus on how the transition state is modified by motion of the metal lattice atoms. These results are used to construct models that explain the strong variation in reactivity with substrate temperature, shown to result primarily from changes in the dissociation barrier height with lattice motion. The dynamics of the dissociative chemisorption of CH₄ on Ni and Pt is explored, using a fully quantum approach based on the reaction path Hamiltonian that includes all 15 molecular degrees of freedom and the effects of lattice motion. Agreement with experiment is good, and vibrational excitation of the molecule is shown to significantly enhance reactivity. The efficacy for this is examined in terms of the vibrationally nonadiabatic couplings, mode softening, mode symmetry, and energy localization in the reactive bond.



I. INTRODUCTION

An important goal of surface science is to understand gas–surface interactions on a molecular level, and by elucidating the mechanisms that underlie heterogeneous catalysis, hopefully design new or better catalysts. We have learned, for example, that the rate-limiting step in many catalyzed reactions is dissociative chemisorption, where one or more of the reactants collide with the surface of the catalyst, breaking a bond. The resulting fragments adsorb onto the surface of the catalyst, becoming mobile intermediates that react to form products. The dissociative chemisorption of N₂ on an Fe-based catalyst is the rate-limiting step in the Haber–Bosch process,¹ the well-known synthesis of ammonia from N₂ and H₂. H₂ also undergoes dissociative chemisorption, and the adsorbed N and H atoms diffuse and react on the catalyst surface.

This article focuses on the dissociative chemisorption of methane, known to be the rate-limiting step in the steam re-forming of natural gas,¹ where CH₄ and H₂O react over a Ni-based catalyst to form CO and 3H₂. This reaction is our primary source for molecular hydrogen, most of which is used in the Haber–Bosch process. Given the obvious industrial and social relevance of these reactions, the dissociative chemisorption of methane has received considerable scientific scrutiny,^{1–4} including numerous molecular beam studies, mostly on Ni^{5–20} and Pt^{20–32} surfaces. These experiments have shown that a single C–H bond breaks as the molecule collides with the surface, leaving chemisorbed H and CH₃ fragments.^{5,30} Electronic structure studies based on DFT (density functional theory) find that the barriers to this reaction are large, on the order of 1 eV for smooth Ni surfaces.^{33–42} As a result, the probability that

methane undergoes dissociative chemisorption as it collides with a bare surface (i.e., the zero-coverage sticking probability, S_0) is small at typical experimental energies, as illustrated in Figure 1 for CH₄ dissociation on Ni(100). We see that S_0 shows a strong increase with both the translational and vibrational energy of the molecule for this highly activated process. Interestingly, this reaction is also significantly enhanced by the thermal energy of the lattice. The variation with temperature is unusually strong for this reaction, and S_0 has been observed to increase by several orders of magnitude with increasing substrate temperature.^{6,9,16,22–24,28,43}

Another interesting aspect of this reaction is that it exhibits nonstatistical behavior with regard to the energy in the incident molecule.^{2–4,8,10–17,19,20,27–30} On Ni(100), for example, adding 0.36 eV to the molecule by exciting the symmetric stretch (ν_1) leads to a greater increase in reactivity than putting the same amount of energy into the incident translational energy,¹⁴ E_i . Adding 0.37 eV by exciting the antisymmetric stretch (ν_3) increases S_0 by a smaller amount than if the same amount of energy were put into translation.⁸ These effects are often expressed in terms of a vibrational efficacy,

$$\eta = \frac{\Delta E_i}{\Delta E_v} = \frac{E_i(0, S_0) - E_i(\nu, S_0)}{\Delta E_v} \quad (1)$$

where ΔE_i is the increase in E_i necessary to give the same S_0 as increasing the vibrational energy by ΔE_v . In eq 1, $E_i(\nu, S_0)$ is the

Received: June 26, 2014

Revised: August 11, 2014

Published: August 25, 2014

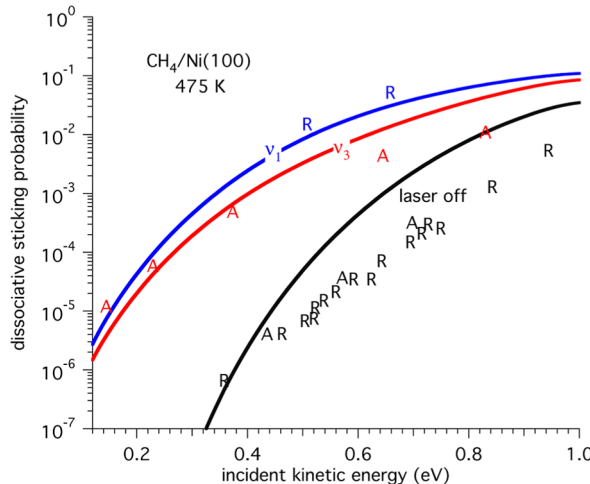


Figure 1. Dissociative sticking probability vs translational energy for CH_4 at normal incidence on $\text{Ni}(100)$. The methane is initially in the ground (black), $1\nu_3$ (red), or $1\nu_1$ (blue) vibrational state. The symbols are experimental data from the groups of Utz⁸ (A) and Beck¹⁴ (R). Reprinted with permission from ref 72 (Figure 8). Copyright 2011 AIP Publishing LLC.

incident translational energy giving S_0 for an initial vibrational state v , and $v = 0$ is the ground state. For dissociation on $\text{Ni}(100)$, $\eta = 1.4$ and 0.94 for the ν_1 and ν_3 excitations, respectively,^{8,14} and if this behavior were purely statistical, one would observe $\eta = 1.0$ for all modes. This is not a small effect; we see in Figure 1 that for $E_i \approx 0.6$ eV, molecules in the ν_1 state are about an order of magnitude more reactive than those in the nearly degenerate ν_3 . Similar nonstatistical behavior has been observed for CH_4 and its isotopologues on several surfaces, and for a given excitation, the efficacy can vary from metal to metal.^{2,3} On $\text{Ni}(111)$, for example, $\eta = 1.25$ for the ν_3 excitation.^{12,13} Bond-selective chemistry has also been observed. For example, in reactions of CD_3H on $\text{Ni}(111)$, excitation of the ν_1 stretch preferentially breaks the C–H bond relative to a C–D bond by a 30:1 ratio.¹⁵ We note that gas-phase reactions of methane with halogen atoms have exhibited similar mode-specific and bond-selective chemistry.^{44–48}

In section II we summarize the results of electronic structure studies of reaction paths and transition states for methane dissociation on several metal surfaces, with a focus on characterizing the molecule–phonon coupling. That is, we explore how the potential energy surface (PES) for the reaction is modified by the motion of the metal atoms. For methane, the lattice relaxes in the presence of the dissociating molecule, and this leads to an unusually strong phonon coupling where the height of the barrier can change with lattice motion. Next, in section III we apply

quantum reactive scattering methods to a low-dimensional model for methane dissociation, showing that our DFT-derived phonon coupling leads to strong variations in S_0 with substrate temperature. These calculations are then used to develop and benchmark more approximate methods that allow us to accurately introduce lattice motion effects into static-lattice calculations. This is important because a quantum treatment of the reaction is preferred, given the low mass of the dissociating H, possible tunneling contributions, and the large amount of zero point energy in the molecule, and explicitly including the motion of one or more heavy lattice atoms in a high-dimensional quantum calculation is prohibitive.

Theory has been hampered by the difficulty of constructing an accurate PES for this reaction, and implementing a quantum reactive scattering calculation that includes all or most of the 15 molecular degrees of freedom (DOFs). Until very recently, studies have been limited to approximate quantum approaches^{23,39–41,43,49–60} or statistical models.^{61–63} In section IV we present a quantum model for the dissociative chemisorption of methane that treats all molecular DOFs, as well as the motion of the lattice, in a reasonable fashion. All parameters describing our PES and the phonon coupling are derived from DFT. This allows, for the first time, a direct comparison with experiment, with all DOFs included and no adjustable parameters or model potentials. We examine the variation of S_0 with incident energy, vibrational state, and substrate temperature, with a focus on the dynamical origins of mode-specific chemistry. In section V we make some connections between our mode-specific studies and similar work in the gas phase, and then close with some conclusions in section VI.

II. TRANSITION STATES AND LATTICE MOTION

We use the DFT-based Vienna *ab initio* simulation package (VASP), developed at the Institut für Materialphysik of the Universität Wien^{64–68} to compute total energies. A supercell with periodic boundary conditions represents our system as an infinite slab, with a large vacuum space above the slab to separate it from its repeated images. The interactions between the ionic cores and the electrons are described by fully nonlocal optimized projector augmented-wave (PAW) potentials,^{68,69} and exchange–correlation effects are treated using the Perdew–Burke–Ernzerhof (PBE) functional.^{70,71} We use four-layer 2×2 supercells, corresponding to methane coverages of $1/4$ monolayer, except for the corrugated $\text{Pt}(110)$ surface, where the slab consists of seven layers. Additional details can be found in our earlier studies.^{42,53,72,73} We use the climbing image-nudged elastic band method^{74,75} to locate all transition states (TSs) and reaction paths.

Table 1 lists properties of transition states for CH_4 dissociation on five surfaces. The geometries are similar: the carbon atom is

Table 1. Properties of Transition States for Methane Dissociative Chemisorption^a

surface	Q (Å)	V^\dagger (eV)	E_a (eV)	Z^\dagger	r^\dagger	θ^\dagger	α	β (eV/Å)
Ni(111)	-0.2	1.33		1.99	1.62	131		
Ni(111)	0	1.08	0.94	2.12	1.60	133	0.70	1.16
Ni(111)	+0.2	0.86		2.27	1.59	136		
Ni(100)	0	0.91	0.78	2.07	1.61	127	0.84	1.19
Pt(100)	0	0.66	0.55	2.26	1.46	136	0.83	1.33
Pt(111)	0	0.93	0.82	2.26	1.49	133	0.83	1.00
Pt(110)-(1×2)	0	0.70	0.60	2.23	1.55	131	0.90	0.76

^a Q is the displacement of the metal atom over which the methane dissociates. The barrier height and the zero-point-energy-corrected barrier height are V^\dagger and E_a , respectively. The distance of the methane center of mass above the surface is Z^\dagger , the length of the dissociating C–H bond is r^\dagger , and the angle of this bond with respect to the surface normal is θ^\dagger . The phonon coupling parameters α and β are defined in the text. Adapted from ref 42.

more or less directly over a top site, with the reacting C–H bond angled toward the surface by about 130° , and stretched by several tenths of an Å from the equilibrium value of 1.1 Å. This late-barrier geometry is consistent with the large increases in S_0 with vibrational excitation. The C–H bond tends to be more elongated at the TS on the Ni surfaces than on the Pt, consistent with the larger efficacies found on this metal.^{2,3} The barrier height V^\dagger is the total energy at the TS minus that for the slab and the molecule at infinite separation, and the activation energy, E_a , is this barrier with all zero point energy corrections. Several methane vibrational modes soften at the TS, lowering the activation energy by about 0.1 eV relative to V^\dagger on all surfaces examined. We find that the barriers are relatively insensitive to the azimuthal orientation of the dissociating C–H bond and the orientation of the nonreacting methyl group,⁴² and recent calculations of CH_4 dissociation on Ni(111) have treated the PES as flat in these variables, with some success.⁷⁶ The values in Table 1 are consistent with other DFT calculations of this nature.^{33–38,77}

If the substrate is allowed to relax in the presence of the dissociating methane, the metal atom over which the molecule dissociates puckers out of the surface by a few tenths of an Å.^{38,39,42,78} Put another way, the height of the barrier to dissociation changes as this metal atom vibrates. This strong molecule–phonon coupling leads to a significant variation of S_0 with substrate temperature T , and similar behavior should be found any time the substrate relaxes significantly during chemisorption. On Ni(111), if we fully relax the metal slab at the TS, the Ni atom directly under the carbon pucks out of the plane of the surface, normal to the surface, by an amount $Q = 0.23$ Å, lowering the barrier by about 0.2 eV.^{38,39} All other lattice distortions are at most a few hundredths of an Å, and thus this strong coupling is limited to this single coordinate Q . We define $Q = 0$ as the equilibrium position for a bare surface, and $Q > 0$ is away from the bulk. In Figure 2 we illustrate the most important

above the surface plane, changes by an amount αQ , where $\alpha = 0.70$. This “mechanical” coupling is how one typically describes the effects of lattice motion on gas-surface scattering: atomic displacements normal to the surface change the location of the repulsive wall in the vicinity of the metal atom. In addition, we see that the barrier height changes by an amount $-\beta Q$, where $\beta = 1.16 \text{ eV}/\text{\AA}$. Additional details on how the TS geometry changes with Q are given in Table 1 for Ni(111), as well as phonon coupling parameters α and β for all surfaces. We observe similar behavior on the other (111) and (100) surfaces examined, and also find that the changes in V^\dagger and Z^\dagger are linear in Q for reasonable values of Q . An exception is the corrugated Pt(110)-(1×2) surface, where several lattice atoms relax in the presence of the methane.⁷³ The value for β in Table 1 corresponds to the largest coupling.

III. THE EFFECTS OF LATTICE MOTION ON DISSOCIATIVE CHEMISORPTION

At the TS the molecule is more-or-less directly over a surface metal atom, and the barriers to dissociation increase rapidly as the point of impact moves away from this top site. Thus, for the most part, energy exchange with the substrate during a reactive collision can be accounted for by considering the motion of this single atom. In addition, nearly all changes in the PES due to lattice motion can be described by Q . An important early model describing these effects, the surface oscillator model (SOM),^{23,43,79} treated methane as the pseudodiatomic RH, keeping the R–H bond parallel to the surface, and only including two DOFs: the R–H bond length r and the distance of the molecule above the plane of the surface, Z . The full particle–lattice PES, V , was constructed from the rigid flat surface PES $V_0(r, Z)$, by writing $V(r, Z, Q) = V_0(r, Z - Q)$. Thus, the barrier to dissociation and the repulsive wall both moved with the metal atom. Computing dissociation probabilities for various initial lattice states and Boltzmann averaging for some T , the SOM successfully reproduced several experimental trends.^{23,43}

Given our DFT studies, we know that the barrier to dissociation does shift with Q , but by an amount αQ , where $\alpha < 1$, and that the barrier height also changes by $-\beta Q$. Our first attempt to incorporate these effects into a quantum scattering calculation also treated the methane as the pseudodiatomic RH but included the polar and azimuthal angles of orientation of the R–H bond, θ and φ , respectively, in addition to r , Z , and the lattice coordinate Q .^{39,40} The PES $V(r, Z, \theta, Q)$, taken to be independent of φ as argued in section II, was fit to our DFT calculations. The location of the molecular center-of-mass over the surface plane (X, Y), was fixed at the top site, and the geometry of the methyl group $R = \text{CH}_3$ evolved adiabatically along the reaction path. Results for the dissociation of CH_4 on Ni(111) are plotted in Figure 3, and the increase in S_0 with substrate temperature T is substantial. The increase is largest at energies below E_a , where the difference in reactivity between a static lattice calculation and a moving lattice calculation can be over 2 orders of magnitude. Even the 0 K and rigid lattice cases differ. At large E_i , the lattice can recoil, lowering the reaction probability. At low E_i , zero-point vibrations of the lattice atoms lead to a lowering of the barrier when $Q > 0$, increasing reactivity.

It is computationally expensive to explicitly include the motion of heavy lattice atoms in a quantum calculation. It is also necessary to repeat such calculations for all initial states of the lattice oscillator reasonably populated at T . We have considered several models to address these issues. Mixed quantum-classical studies using the PES in the preceding paragraph, but treating

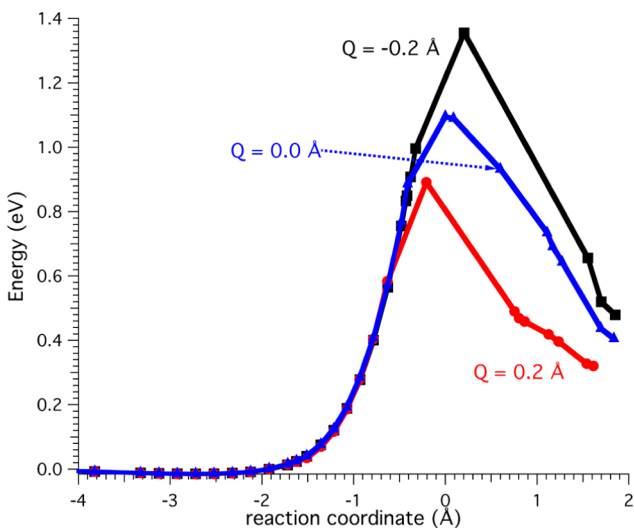


Figure 2. Energy along the minimum energy path for the dissociative chemisorption of CH_4 on Ni(111), for different values of Q , the displacement of the lattice atom from equilibrium. The curves are shifted so that the asymptotic energies are all zero.

changes in the PES due to lattice motion, plotting minimum energy paths (MEPs) for dissociation on Ni(111) for three fixed values of Q . As this lattice atom vibrates, the location of the transition state along Z , the distance of the CH_4 center of mass

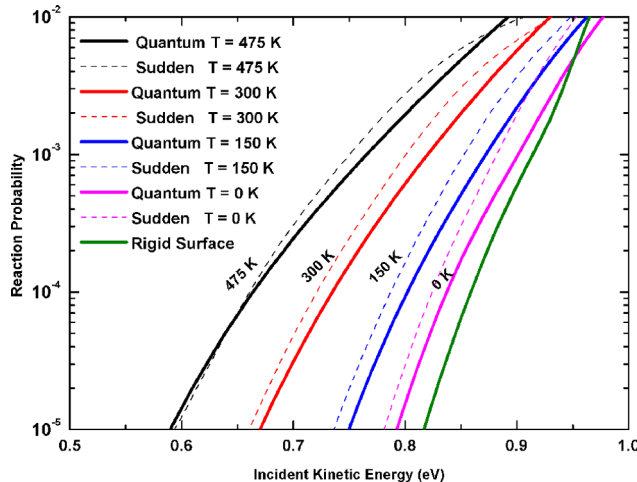


Figure 3. Reaction probabilities for CH_4 on $\text{Ni}(111)$ vs incident energy for four substrate temperatures T . The solid lines are the quantum results for our 5-DOF model, and the dashed lines are from the sudden approximation. The green curve is for a rigid lattice. Reprinted with permission from ref 52 (Figure 4). Copyright 2009 American Physical Society.

Z and Q classically, showed that the lattice atom did not move significantly during the collision,^{52,54} suggesting that a sudden treatment of the lattice should be valid. In Figure 3 are plotted the results of such a calculation, where lattice displacements Q are sampled from a Boltzmann distribution at the substrate temperature, and for each value of Q a fully quantum calculation is implemented treating r , Z , θ , and φ as above, but holding Q fixed. These sudden results compare well with the exact quantum calculations, over several orders of magnitude and a wide range of T . We note that for a classical sampling of Q at 0 K, $Q = 0$ only and the sudden results would normally be equal to the rigid lattice results. Instead, for this 0 K case only, we set the Q distribution equal to the square of the ground state vibrational wave function, leading to better agreement. Our approach reduces computational time by over an order of magnitude. One can get similar results with even less effort by using an “energy-shifting” approximation. Assuming that the morphology of the PES does not change significantly with Q , except for a rescaling of the barrier height, the reaction probability for $Q \neq 0$ should be similar to that for $Q = 0$, $P_0(E_i)$, but shifted along the E_i axis by an amount equal to the change in barrier height, $-\beta Q$. The temperature dependent dissociative sticking probability due to the β -coupling, $S_\beta(E_i; T)$, is thus

$$S_\beta(E_i; T) = \sqrt{\frac{M_s \Omega^2}{2\pi kT}} \int_{-\infty}^{\infty} e^{-M_s \Omega^2 Q^2 / 2kT} P_0(E_i + \beta Q) dQ \quad (2)$$

where M_s and Ω are the mass and vibrational frequency of the lattice atom, respectively. This approach gives results similar^{52,54} to the sudden case in Figure 3.

We further improve these sudden models by averaging over P as well as Q , where P is the lattice atom momentum conjugate to Q . This amounts to including the mechanical (α) coupling. We use a modified form of the surface mass model (SMM),⁴³ developed to introduce much of the physics of the SOM into the results of rigid lattice calculations. For some $Q = Q_0$, we approximate our model PES as $V(Z - \alpha Q, r, \theta; Q_0)$, where we have introduced the mechanical coupling as in the SOM, except that $\alpha \neq 1$. We then transform Z and Q to a relative coordinate $Z' = Z - \alpha Q$

and a corresponding center-of-mass coordinate. Our derivation⁵⁴ is similar to that of the SMM,⁴³ except that the reduced mass corresponding to the relative collision coordinate Z' is $\mu_r = M'_s M / (M'_s + M)$, where M is the molecular mass and $M'_s = M_s / \alpha^2$. Implementing a quantum scattering calculation for the PES $V(Z', r, \theta; Q_0)$, the computed reaction probability, $P_{\text{rel}}(E_{\text{rel}}; Q_0)$, corresponds to the relative collision energy^{43,54} E_{rel} :

$$E_{\text{rel}} = \frac{1}{2} \mu_T \left(\sqrt{\frac{2E_i}{M}} - \alpha \frac{P}{M_s} \right)^2 \quad (3)$$

One can then compute the temperature-dependent dissociative sticking probability with the α -coupling, S_α for a given E_i and Q_0 , by averaging this over a Boltzmann distribution for P .^{43,54} It is useful to convert the integral over P into one over E_{rel} , giving

$$S_\alpha(E_i; T, Q_0) = \int dE_{\text{rel}} \sqrt{\frac{M'_s}{4\pi kT\mu_T E_{\text{rel}}}} \exp\left(-\frac{M'_s}{2kT} \left(\sqrt{\frac{2E_{\text{rel}}}{\mu_T}} - \sqrt{\frac{2E_i}{M}} \right)^2\right) P_{\text{rel}}(E_{\text{rel}}; Q_0) \quad (4)$$

In practice, we include both the mechanical coupling (α) and the energetic coupling (β) by combining eqs 2 and 4, averaging our rigid-lattice reaction probability over both P and Q . The resulting reaction probabilities for $\text{Ni}(111)$ at $T = 475$ K and for $\text{Pt}(111)$ at $T = 600$ K are compared with fully quantum results (using our 5-DOF model) in Figure 4. The agreement is excellent.

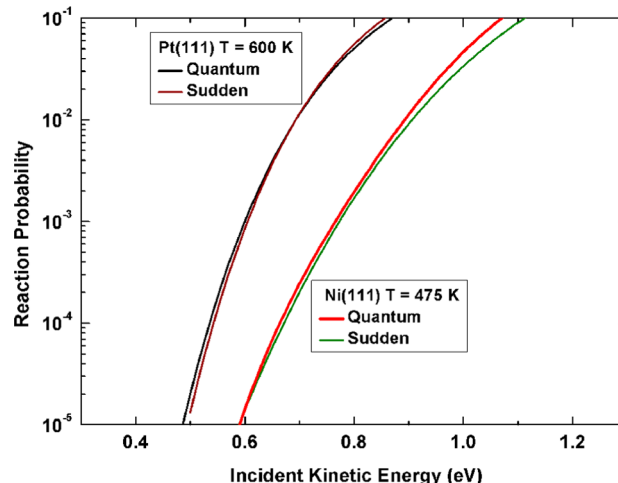


Figure 4. Dissociation probabilities for CH_4 vs incident energy. Results are shown for both the fully quantum calculation and the sudden approximation with α and β coupling. Reprinted with permission from ref 54 (Figure 11). Copyright 2010 AIP Publishing LLC.

For $\text{Pt}(111)$, α is larger than for $\text{Ni}(111)$, and it is particularly important to include the mechanical coupling. It is thus possible to accurately introduce the effects of lattice motion into rigid lattice calculations, once the coupling parameters α and β have been computed.

IV. REACTION PATH MODELS FOR DISSOCIATIVE ADSORPTION

To explore the dynamics of mode-specific chemistry, we need an approach that accurately models the various bends and stretches of the molecule. A quantum treatment is preferred, given the small effective masses of these vibrations and the correspondingly large

vibrational spacings and zero point energies. Also, much of the experimental data is at incident energies below the rigid-lattice E_a , as computed by DFT (Figure 1). S_0 is small at these energies, and tunneling may be important. We have had success with an approach based on the reaction path Hamiltonian^{80,81} (RPH), where the PES is approximated as harmonic with respect to displacements away from the reaction path, or MEP. The RPH has had many applications, particularly to transition state theory calculations of rate constants involving polyatomic molecules.⁸² It has also been used in several dynamical studies,^{83–89} often involving semiclassical or mixed quantum-classical approximations. To our knowledge, this is the first attempt to use the RPH to implement a fully quantum reactive scattering calculation involving a polyatomic molecule.

For a rigid surface, our Hamiltonian is

$$H = K + V = -\frac{\hbar^2}{2} \sum_{i=1}^{15} \frac{\partial^2}{\partial x_i^2} + V(x_1, x_2, \dots, x_{15}) \quad (5)$$

where x_i are the mass-weighted Cartesian coordinates of the CH₄ nuclei. To construct V , we first locate the MEP. The distance along this path is s , where $(ds)^2 = \sum_{k=1}^{15} (dx_k)^2$. At numerous points along s we compute the total energy, $V_0(s)$. A normal-mode analysis at these points provides the 14 normal vibrational coordinates Q_k and corresponding frequencies $\omega_k(s)$ that describe displacements orthogonal to the reaction path at s , in the harmonic approximation. Our PES, in the reaction path coordinates s and $\{Q_k\}$ is

$$V = V_0(s) + \sum_{k=1}^{14} \frac{1}{2} \omega_k^2(s) Q_k^2 \quad (6)$$

Our first approximation is thus to ignore any anharmonic terms in V . The quantities defining V are plotted in Figure 5 for CH₄ on

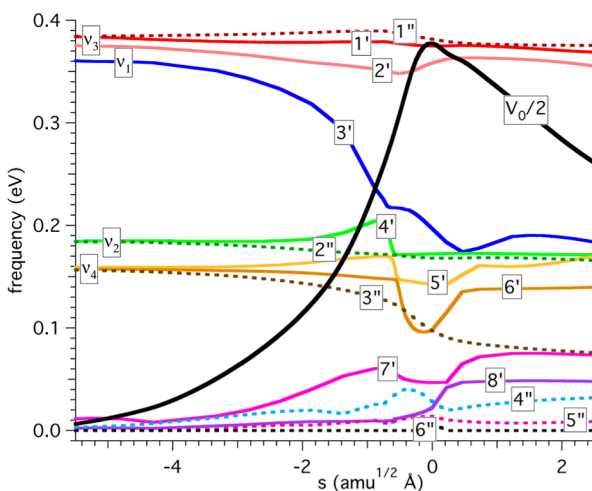


Figure 5. Energies of the 14 normal modes of CH₄, along the reaction path s , for dissociation on Ni(100). The eight vibrations with A' symmetry are labeled 1'-8', and the six modes with A'' symmetry are labeled 1''-6''. The energy along the MEP is also plotted, scaled by one-half. Reprinted with permission from ref 72 (Figure 1). Copyright 2011 AIP Publishing LLC.

Ni(100). When the molecule is far above the surface (large negative s), nine of the frequencies are nonzero: the triply degenerate antisymmetric stretch, ν_3 , the symmetric stretch, ν_1 , the doubly degenerate bend, ν_2 , and the triply degenerate bend, ν_4 .

The interaction with the surface removes these degeneracies and softens the symmetric stretch and some of the bends near the transition state, $s = 0$. As noted, one consequence of this softening is that zero point energy (ZPE) corrections lower the barrier heights by about 0.1 eV.⁴² The remaining five frequencies are zero at large negative s , where they correspond to molecular rotation and translation parallel to the surface. As the molecule approaches the surface, these modes become hindered rotations and translations and eventually mix with internal types of motion. The reaction path is symmetric with respect to reflection through a plane that lies perpendicular to the surface and along the dissociating C–H bond, and the normal modes are either symmetric (A') or antisymmetric (A'') with respect to reflection through this plane. We label the A' modes 1'-8' and the A'' modes 1''-6''.

The eigenvectors from our normal mode calculations, $L_{i,k}(s)$, define the transformation between the x_i and our reaction path coordinates:

$$x_i = a_i(s) + \sum_{k=1}^{14} L_{i,k}(s) Q_k \quad (7)$$

where the $a_i(s)$ give the configuration of the molecule on the reaction path at point s . Changing K to our reaction path variables, the quantum form of our Hamiltonian can be written⁸¹ $H = K_1 + K_2 + V$, where

$$K_1 = \frac{1}{2} \sum_{k=1}^{14} (1 + b_{ss})^{-1/2} P_k (1 + b_{ss}) P_k (1 + b_{ss})^{-1/2} \quad (8)$$

and

$$K_2 = \frac{1}{2} (1 + b_{ss})^{-1/2} (p_s - \pi_s) (1 + b_{ss})^{-1} (p_s - \pi_s) (1 + b_{ss})^{-1/2} \quad (9)$$

The momenta conjugate to s and Q_k are p_s and P_k respectively, and

$$b_{ss} = \sum_{k=1}^{14} Q_k B_{k,15}(s) \quad \text{and} \quad \pi_s = \sum_{k=1}^{14} \sum_{j=1}^{14} Q_k P_j B_{k,j}(s) \quad (10)$$

The vibrationally nonadiabatic couplings are given by

$$B_{k,j}(s) = \sum_{i=1}^{15} \frac{dL_{i,k}}{ds} L_{i,j}(s) \quad (11)$$

One can show that

$$\begin{aligned} K_1 &= \frac{1}{2} \sum_{k=1}^{14} \left[P_k^2 - \frac{\hbar^2}{4} (1 + b_{ss})^{-2} B_{k,15}^2 \right] \\ &= \frac{1}{2} \sum_{k=1}^{14} P_k^2 - \frac{\hbar^2 \kappa^2}{8} (1 + b_{ss})^{-2} \end{aligned} \quad (12)$$

where $\kappa(s)$ is the curvature.⁸¹ In practice, we expand both K_1 and K_2 in a power series in b_{ss} :

$$\begin{aligned} H = H_{\text{vib}} + V_0(s) + \frac{1}{2} p_s^2 - \frac{1}{4} (b_{ss} p_s^2 + 2 p_s b_{ss} p_s + p_s^2 b_{ss}) \\ - \frac{1}{2} (p_s \pi_s + \pi_s p_s) + \dots \end{aligned} \quad (13)$$

where

$$H_{\text{vib}} = \sum_{k=1}^{14} \left[\frac{1}{2} P_k^2 + \frac{1}{2} \omega_k^2(s) Q_k^2 \right] \quad (14)$$

In eq 13, although we only show terms up to first order in the nonadiabatic couplings, we will eventually include all terms through second order in the $B_{k,15}$. The operator π_s describes energy flow between all modes k and j , through the Coriolis couplings $B_{k,j}$. The operator b_{ss} describes energy flow between the vibrational modes k and motion along the reaction coordinate, due to the curvature, with couplings $B_{k,15}$. Our “15th eigenvector” is the normalized gradient vector describing motion along the MEP (the “mode” with the imaginary frequency at the TS). The symmetry is important, as the $B_{k,j}$ ’s only couple modes of the same symmetry, and because the reaction path is symmetric, $B_{k,15} = 0$ for the A'' modes.

We use a close-coupled wave packet approach to describe our total molecular wave function, writing

$$\Psi(t) = \sum_n \psi_n(s, \{Q_k\}_u; t) \Phi_n(\{Q_k\}_b; s) \quad (15)$$

where $\{Q_k\}_b$ are the normal coordinates of the nine vibrational modes that are bound at large negative s , and $\{Q_k\}_u$ are the five that are unbound ($\omega_k = 0$). The Φ_n are eigenfunctions of that part of H_{vib} corresponding to the asymptotically bound modes ($1' - 6'$ and $1'' - 3''$), with eigenvalues $\sum_k^{\text{bound}} \hbar \omega_k(s) (n_k + \frac{1}{2})$ and quantum numbers $\mathbf{n} = \{n_k\}_b$. These vibrationally adiabatic Φ_n are thus products of one-dimensional harmonic oscillator eigenfunctions that depend parametrically on s . Asymptotically, the $\{Q_k\}_u$ describe rotation of the molecule and motion along X and Y away from the MEP. In the entrance channel and up to the transition state, X and Y remain almost directly over the top site, corresponding to $X = 0$ and $Y = 0$ in our coordinate system. It is reasonable to assume that motion along X and Y is slow on collision time scales, given the relatively large total molecular mass, the large collision energies, and our normal incidence conditions. We thus implement our scattering calculation for fixed values X_0 and Y_0 , fixing the corresponding $\{Q_k\}_u$ and setting their $P_k = 0$ in eq 9. We then average the resulting reaction probabilities over all impact sites (X_0, Y_0) on the surface unit cell. The remaining $\{Q_k\}_u$ describe molecular rotation in the entrance channel. The rotational temperature in the molecular beams is low, about 10 K, and we assume that the molecule is initially in the ground rotational state. Experiment suggests that moderate rotational excitation of the incident molecule does little to modify the reactivity⁹⁰ and given the spherical shape of CH₄, the collision should not lead to significant rotational excitation. As the molecule approaches the metal, there are always one or more H atoms pointing toward the surface, and only minor angular reorientation should be required to enter the transition state. Given this, and the fact that the moment of inertia is relatively small, it is tempting to assume that there is a reasonable amount of rotational steering, and we assume rotational adiabaticity, writing

$$\psi_n(s, \{Q_k\}_u; t) = \chi_n(s; X_0, Y_0; t) R_0 \quad (16)$$

where R_0 is the ground state eigenfunction of that part of the Hamiltonian containing the remaining $\{P_k, Q_k\}_u$.

Given our total wave function in eqs 15 and 16, and our Hamiltonian of eq 13, the time-dependent Schrödinger equation leads to coupled equations of motion⁷² for the wave packets, $\chi_n(s; X_0, Y_0; t)$. We consider first the simple case where the expansion

in eq 15 includes only the vibrational ground state and the nine singly excited states corresponding to one quantum of energy in one of the asymptotically bound modes. Consistent with this, we truncate our Hamiltonian to first order in b_{ss} and π_s . The resulting equations of motion are⁷²

$$i\hbar \frac{\partial \chi_0(s; X_0, Y_0; t)}{\partial t} = \left(\frac{1}{2} p_s^2 + V_{\text{eff},0} + \Delta V \right) \chi_0 + \sum_v \left[f_v \frac{\partial^2 \chi_v}{\partial s^2} + \frac{df_v}{ds} \frac{\partial \chi_v}{\partial s} + \frac{1}{4} \frac{d^2 f_v}{ds^2} \chi_v \right] \quad (17)$$

$$i\hbar \frac{\partial \chi_v(s; X_0, Y_0; t)}{\partial t} = \left(\frac{1}{2} p_s^2 + V_{\text{eff},v} + \Delta V \right) \chi_v + \left[f_v \frac{\partial^2 \chi_0}{\partial s^2} + \frac{df_v}{ds} \frac{\partial \chi_0}{\partial s} + \frac{1}{4} \frac{d^2 f_v}{ds^2} \chi_0 \right] + \sum_{v'} \left[g_{vv'} \frac{\partial \chi_{v'}}{\partial s} + \frac{1}{2} \frac{dg_{vv'}}{ds} \chi_{v'} \right] \quad (18)$$

where the subscript 0 denotes the vibrationally adiabatic ground state and $v = 1' - 6'$ or $1'' - 3''$ labels the excited states. The wave packets evolve on the coupled effective (vibrationally adiabatic) potentials

$$V_{\text{eff},n}(s) = V_0(s) + \sum_{k=1}^{14} \hbar \omega_k(s) \left(n_k + \frac{1}{2} \right) \quad (19)$$

where $V_{\text{eff},0}$ is simply the MEP with ZPE corrections. The barrier height on the ground state ZPE-corrected MEP is about 0.78 eV. Note how mode softening, in addition to lowering E_a relative to V^\ddagger by 0.13 eV, leads to different barrier heights on different V_{eff} . This effect is largest for the symmetric stretch ($v = 3'$), and thus $V_{\text{eff},3'}$ has the smallest barrier. The term $\Delta V(s; X_0, Y_0)$ modifies the reaction path according to the surface impact site (X_0, Y_0) . The coupling functions in eqs 17 and 18 are given by

$$f_v(s) = \hbar^2 \sqrt{\frac{\hbar}{2\omega_v(s)}} B_{v,15}(s) \quad (20)$$

and

$$g_{vv'}(s) = \frac{\hbar^2}{2} \left[\sqrt{\frac{\omega_{v'}(s)}{\omega_v(s)}} B_{v,v'}(s) - \sqrt{\frac{\omega_v(s)}{\omega_{v'}(s)}} B_{v',v}(s) \right] \quad (21)$$

The parametric dependence of the Φ_n on s results in couplings that depend upon the momentum and kinetic energy of the molecule, and curve crossing becomes increasingly likely at higher velocities, as well as larger $B_{v',v}$. Consistent with our treatment of the $\{Q_k\}_u$, we neglect terms describing energy flow between the unbound and bound modes.

To compute the dissociative sticking probability, we first solve eqs 17 and 18 for some initial vibrational state \mathbf{n}_0 , and for $X_0 = Y_0 = 0$, corresponding to dissociation over the top site, where the barrier is lowest ($\Delta V = 0$). Initially, all of the wave packets χ_n are zero, except for the one corresponding to \mathbf{n}_0 , which is centered far above the surface. Standard techniques^{72,91} are used to propagate the wave packets in time, and the reactive flux at large positive s is Fourier transformed in time on each channel \mathbf{n} , giving both vibrational state-resolved and energy-resolved reaction probabilities for all incident energies E_i included in the initial wave packet.^{92,93} The resulting rigid-surface single-impact-site

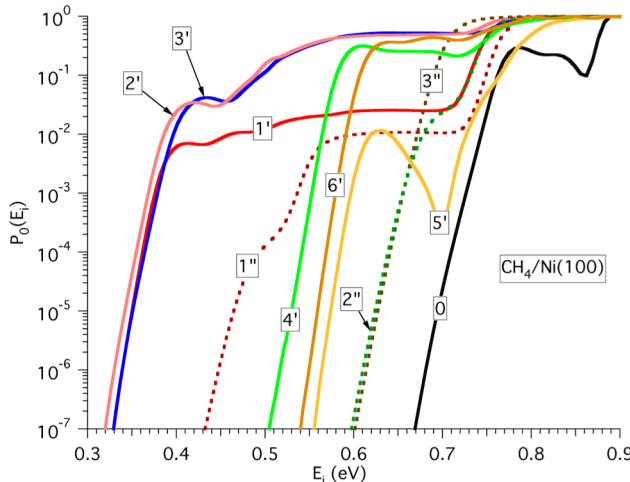


Figure 6. Rigid-surface single impact site reaction probabilities vs incident energy, for CH₄ dissociation on Ni(100). The black curve labeled “0” is for the ground vibrational state, and the excited states are labeled using the color scheme and notation of Figure 5. Reprinted with permission from ref 72 (Figure 6). Copyright 2011 AIP Publishing LLC.

reaction probabilities, $P_0(E_i, \mathbf{n}_0; X_0=Y_0=0)$, are plotted in Figure 6, for CH₄ incident on Ni(100). The structure is easily understood in terms of the vibrationally adiabatic potentials and the non-adiabatic couplings $B_{k,15}$ and B_{kj} . Consider, for example, the $1'$ state, where the barrier along $V'_{\text{eff},1}$ is roughly that of the ground state potential, 0.78 eV, given the lack of mode softening. In the absence of nonadiabatic coupling ($B_{k,15} = B_{kj} = 0$), P_0 for molecules initially excited to the $1'$ state should decrease rapidly for energies below 0.78 eV, as tunneling becomes the only mechanism for reaction. We see this clearly in Figure 6. However, inclusion of the curvature coupling $B_{1',15}$ allows for transitions to the vibrationally adiabatic ground state, making over-the-barrier processes possible down to $E_i \approx 0.4$ eV. This is the origin of the shoulder in the $1'$ reaction probability between 0.4 and 0.78 eV. Below $E_i \approx 0.4$ eV tunneling is the only possible rigid-lattice reaction mechanism, and the reaction probability drops rapidly with decreasing energy. Thus, the curvature coupling $B_{k,15}$, converts the energy placed (asymptotically) into vibrational motion into motion along the reaction path, and as expected for this late barrier system these couplings become large before the barrier. At the TS, this motion corresponds to bond breaking. As a result, we see in Figure 6 that the A' states are typically more reactive than the A'' states, taking the initial vibrational energy in these states into consideration. Molecules excited to the $3'$ state are particularly reactive, as mode softening allows for direct processes, even without nonadiabatic transitions, down to $E_i = 0.62$ eV. In addition of the three A' stretching modes, the symmetric stretch ($3'$) has the largest curvature coupling, and its probability in the shoulder region, between 0.4 and 0.6 eV, is much larger. Interestingly, the $2'$ reactivity is also large, as the Coriolis coupling $B_{2',3'}$ mixes these states in the entrance channel.

To compute the final sticking probability, we average $P_0(E_i, \mathbf{n}_0; X_0=Y_0=0)$ over impact sites X_0 and Y_0 in the surface unit cell and include the effects of lattice motion. We use the following “energy-shifting” approximation to estimate P_0 for impacts away from the top site ($X_0 = Y_0 = 0$):

$$P_0(E_i, \mathbf{n}_0; X_0, Y_0) \approx P_0[E_i - \Delta V(X_0, Y_0), \mathbf{n}_0; X_0 = Y_0 = 0] \quad (22)$$

where ΔV is the increase in barrier height at (X_0, Y_0) relative to the top site. Using eqs 6 and 7, we write ΔV for a displacement ΔX away from the reaction path at the TS as

$$\begin{aligned} \Delta V &= \frac{1}{2} \sum_{k=1}^{14} \omega_k^2 Q_k^2 = \frac{1}{2} \sum_{i=1}^{14} \left(\sum_{j=1}^5 \sqrt{m_j} L_{3i-2,j} \right)^2 \omega_k^2 \Delta X^2 \\ &= \frac{1}{2} M \Omega_X^2 \Delta X^2 \end{aligned} \quad (23)$$

where the m_i are the atomic masses and the sum over i includes only the x -coordinates of the five atoms. Equation 23 describes a lateral translation of the entire molecule by ΔX , without relaxing the TS geometry otherwise, and we use the $s=0$ values for ω_k and $L_{i,k}$. Displacement along X is orthogonal to our symmetry plane, and the sum over k is dominated by the asymptotically unbound A'' modes ($4'', 5'',$ and $6''$), which combine to give $\hbar \Omega_X = 0.023$ eV. Computing ΔV for a displacement ΔY , we find that several of the A' modes contribute to give $\hbar \Omega_Y = 0.012$ eV. The effect of averaging P_0 over impact sites in the surface unit cell is large, as illustrated in Figure 7. The barrier increases rapidly as

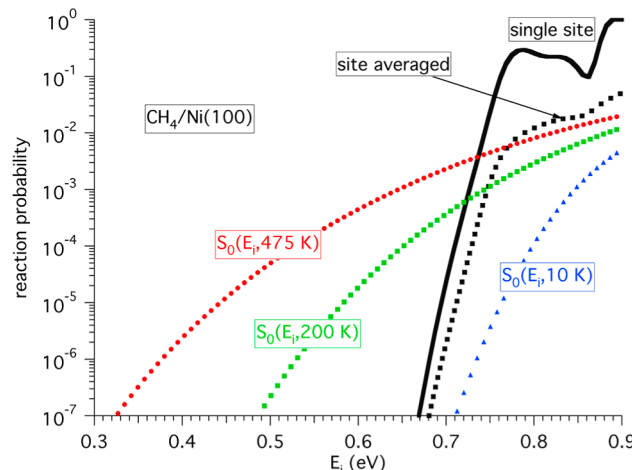


Figure 7. Reaction probability vs collision energy for methane initially in the ground vibrational state. Results are shown for the single-site rigid lattice case (solid), for the site-averaged rigid-lattice case (dotted), and for the dissociative sticking probabilities at 10, 200, and 475 K, which include the effects of site averaging and lattice motion.

the molecule moves away from the top site, and the net effect is to lower the reaction probability by an order of magnitude or more, at all energies. Finally, we use eqs 2 and 4 to introduce the effects of lattice motion, and the result is the dissociative sticking probability, $S_0(E_i, \mathbf{n}_0, T_s)$, plotted in Figure 7 for three substrate temperatures. The effects are substantial. At very low temperatures, the reaction probability is actually lowered due to lattice recoil. As the substrate temperature increases, S_0 increases by several orders of magnitude. In fact, without the inclusion of lattice motion, the sticking probability is basically zero below about 0.7 eV. With lattice motion, reaction becomes possible for these low energies at puckered sites on the surface, where the barrier is lowered. Effects due to the relative collision velocity (the SOM and SMM models) are also important. We note that although eq 2 assumes a harmonic potential for motion of the lattice atom, anharmonic effects are important,⁹¹ as it is easier for a metal atom to move away from the bulk than into the bulk. For all results presented in this article, we use DFT to compute the energy required to distort the metal lattice, and use that in eq 2.

In Figure 1 we plot our computed S_0 for CH_4 dissociation on Ni(100), along with experimental data from the Utz and Beck groups. The agreement with experiment is good with regard to the variation in S_0 with incidence energy and initial vibrational state. In particular, the method is able to reproduce the larger efficacy η for the ν_1 symmetric stretch relative to the ν_3 antisymmetric stretch. The origin of this difference, within our RPH model, can be seen in Figure 6. The $2'$ and $3'$ modes couple and mix and are both very reactive at the low incidence energies of the experiment due to the $3'$ mode softening and efficient curvature coupling. The $1'$ is less reactive than either of these modes due to smaller coupling, as discussed, and the $1''$ can only convert its asymptotic vibrational energy into motion along the reaction path by coupling to the $2''$ and $3''$ states, because $B_{k,15} = 0$ by symmetry. Because the ν_3 state includes these two less reactive modes, the efficacy is lower than for the ν_1 state. It is clear from Figure 7 that the comparison with experiment would be off by several orders of magnitude without the introduction of lattice motion effects. Our model does give too large a sticking for ground state methane, particularly at high energies. This is perhaps due to our use of the PBE functional, believed to give barriers that are too small,^{94,95} or our adiabatic treatment of rotational motion, which is likely to overestimate S_0 . Thus, though S_0 is larger for ν_1 than ν_3 , the numerical values for η are smaller than the experimental values.

Overall, the agreement with experiment is probably better than one might expect, considering the relative simplicity of the model. Once the MEP is located and the normal modes computed, the computation of S_0 at all energies for a particular initial vibrational state requires only a few seconds on a single processor, because the problem is reduced to the propagation of 10 coupled one-dimensional wave packets. Perhaps more important than a rigorous agreement with experiment is that we have a reasonable and fully quantum model for reaction dynamics in the presence of a bath, which lets us easily examine how energy moves among the various DOFs during a reaction. All components of the PES, and all parameters used to introduce the effects of averaging over lattice motion and impact site can be derived from first principles. The approach easily models a five-atom system, and the addition of several more molecular or lattice DOFs would not make the computation intractable.

We have examined methane reactions on two other metal surfaces. In Figure 8 we plot S_0 for CH_4 incident on Ni(111), for two different basis sets. The dashed lines correspond to our original calculation,⁹¹ where the sum over n in eq 15 is limited to the ground state and the nine singly excited vibrational states, and H is truncated to first order in b_{ss} and π_s . The solid lines in Figure 8 correspond to calculations where we significantly extend our basis set to include in Ψ all 45 doubly excited states of the molecule.⁹⁶ Correspondingly, we have expanded H to include all two-quanta terms: second order in b_{ss} and first order in π_s . The resulting equations contain many coupling terms⁹⁶ and are not reproduced here, but the physics is similar: b_{ss} links states that differ by one vibrational quantum and π_s couples states that differ by two quanta, both vibrational states being of the same symmetry. However, we find that including terms beyond first order in the $B_{k,15}$ does not significantly modify the results, particularly after averaging over impact sites and lattice motion.⁹⁶ Unless otherwise noted, the results in the remainder of this article correspond to our first-order H and the larger vibrational basis (55 states).

In Figure 8 we see that although inclusion of the larger basis allows for the treatment of two-quanta excited states, it does not appreciably change our earlier results for one-quantum initial states.

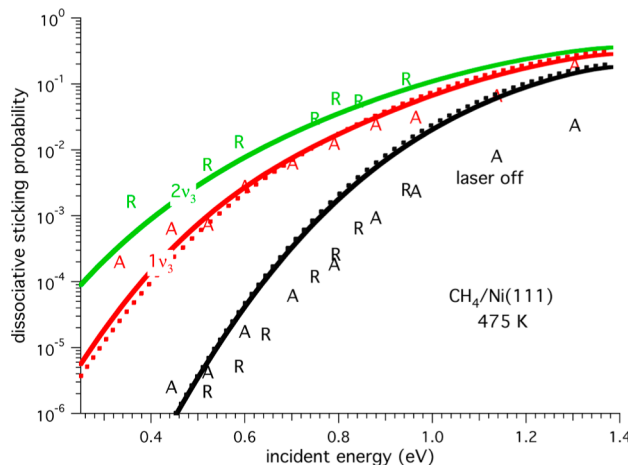


Figure 8. Dissociative sticking probability vs incident energy, for CH_4 dissociation on Ni(111). Methane is initially in the ground (black), $1\nu_3$ (red), or $2\nu_3$ (green) vibrational states. Results are shown for both the small (dashed lines) and large (solid lines) basis sets. Symbols are experimental data from the groups of Utz¹² (A) and Beck (R).²⁰ Reprinted with permission from ref 96 (Figure 4). Copyright 2014 AIP Publishing LLC.

As for our Ni(100) calculations, the RPH model accurately describes the dissociative sticking for the two excited states, and their relative reactivity, but overestimates the ground state reactivity at high incidence energies. We note that the PES and nonadiabatic couplings for Ni(111) are very similar to those on Ni(100), except for the lower barrier height on Ni(100). Overall, the results are satisfying and we can understand the large efficacies for the ν_3 and $2\nu_3$ stretching states in terms of the effective potentials and nonadiabatic couplings,⁹⁶ as for Ni(100). The temperature effects are also large, and similar to those on Ni(100), as suggested by the phonon couplings in Table 1. In fact, the Utz group has been able to measure S_0 on Ni(111) as a function of temperature,^{4,16} providing an opportunity to better understand how lattice motion modifies the reaction dynamics, as well as to test our models. In Figure 9 we plot their results for

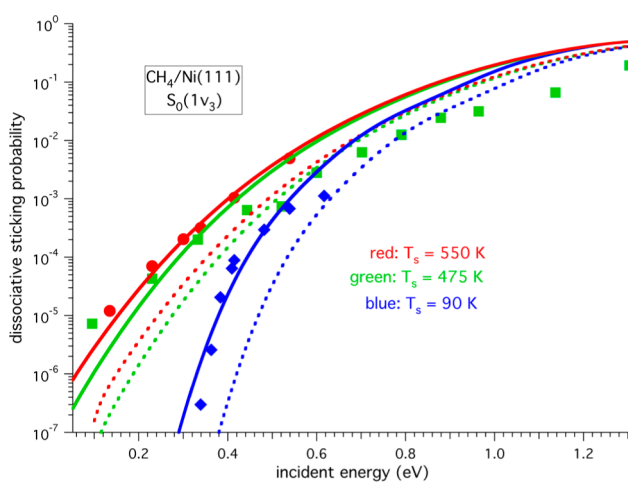


Figure 9. Dissociative sticking probability for methane initially in the $1\nu_3$ vibrational state, as a function of incident energy and substrate temperature. The dashed lines are theory, and the symbols are experimental data from the Utz group.⁴ The solid lines are the theory shifted along the energy axis to better align with the data. Reprinted with permission from ref 91 (Figure 6). Copyright 2013 AIP Publishing LLC.

CH_4 molecules initially in the $1\nu_3$ state, along with the results of our calculation. We see that the variation with temperature is well described by our lattice-sudden model. Our ZPE-corrected ground state barrier height is 0.94 eV, roughly the same as the vibrationally adiabatic barriers for the 1', 2', and 1'' modes that make up the $1\nu_3$ state. Given the asymptotic energy of the $1\nu_3$ stretch, 0.38 eV, over-the-barrier reaction is energetically possible for incident energies above 0.56 eV, without the need for lattice motion. Thus, in our model the increase in sticking with temperature is relatively weak above about 0.56 eV, where the reaction probability begins to saturate. At E_i below this, the variation with temperature is strong, as lattice motion is necessary to make the reaction energetically feasible without the need for tunneling. At very low substrate temperatures, where the thermal effects are weak, the decrease in reactivity with decreasing incident energy is rapid, as molecules can only dissociate via tunneling. Indeed, the slopes of both the experimental and theory results at 90 K are similar to the slopes of the rigid lattice reaction probabilities in Figure 6, at low incident energies where tunneling dominates. Given errors in the PES and the model, our computed curves in Figure 9 are shifted to higher energies relative to experiment. To better focus on how S_0 varies with T , we replot our results, shifting them along the energy axis by 0.09 eV to better align with the experimental data. It is clear that our model accurately reproduces the variation in S_0 with T , including how this behavior differs above and below E_a .

The dissociative chemisorption of methane on Pt(110)-(1×2) has been studied by several groups.^{25,26,28,29,32,42,77,97,98} Pt(110) undergoes a missing row reconstruction, leaving rows of “exposed” Pt atoms on the surface separated by large troughs, two atomic layers deep. This surface thus serves as a model for real catalysts, which are rough, and where reactions are likely to take place at edge sites. Indeed, we have identified 4 TSs for dissociation on this surface,^{42,73} and all are over Pt atoms on the exposed ridge, with relatively low activation energies of about 0.6 eV (Table 1). We are also interested in how the phonon coupling and lattice motion might differ at these edge sites. Though the vibrational amplitudes of the substrate atoms are not significantly different, the motion of several of these metal atoms can modify the barrier height. That is, lattice relaxation in the presence of the dissociating molecule involves several atoms. We constructed a RPH for this surface and computed S_0 , modifying eq 2 to include several oscillators.⁷³ There are six major couplings β in the range 0.3–0.8 eV/Å, and many weaker ones.⁷³ We find that the overall effects are similar to those on the close-packed surfaces; the couplings are weaker but there are many of them, though multiple contributions tend to add out of phase. In Figure 10 we plot our results along with experimental data from the Beck group.²⁸ The agreement with respect to both the magnitude of the sticking and the variation with T is good, considering the complexity of the system. As in our studies on Ni, the model tends to overestimate the reactivity at saturation. The increase in reactivity with T is again strongest at lower E_i for both experiment and theory, and the computed magnitude of this increase is in good agreement with the data of Beck and co-workers. The experiments were performed with a nozzle temperature T_n in the range 323–373 K, and this can affect the results at low E_i . The vibrational state distribution in the beam is roughly Boltzmann at T_n , and we have found⁹¹ that at low incident energies, small populations of highly reactive vibrationally excited molecules can make a significant contribution to S_0 . For Pt(110)-(1×2) we have not computed sticking probabilities for all of the many excited states populated at T_n , and experimental

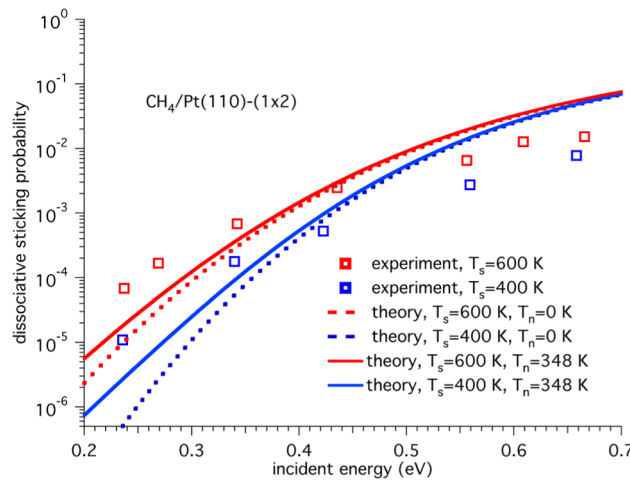


Figure 10. Dissociative sticking probabilities on Pt(110)-(1×2), for methane initially in the ground vibrational state, as a function of incident energy, substrate temperature T , and nozzle temperature T_n . The lines are theory, and the symbols are experimental data.²⁸ Reprinted from ref 73.

efficacies are not known for most of these states. However, we can estimate the T_n effects⁹¹ by assuming a vibrational efficacy of 0.7 for every excited state and approximate the sticking for an excited state n , with energy E_n , as $S_0(E_n, T_s) \approx S_0(E_i + 0.7E_n, 0, T_s)$, where $S_0(E_i, 0, T_s)$ is our computed ground state sticking probability. The results for $T_n = 348$ K, the average experimental value, are also plotted in Figure 10. We see that adding these nozzle temperature effects tends to lower the enhancement in reactivity with increased substrate temperature, as a larger percentage of the reactivity results from vibrationally excited molecules that are closer to the saturation value of S_0 . Agreement with experiment at lower incident energies is significantly improved. Our models for including the effects of lattice motion work well for this system, though many types of lattice motion need to be included.

In Figure 11 we examine more closely how the two components of the phonon coupling modify the dissociative sticking.

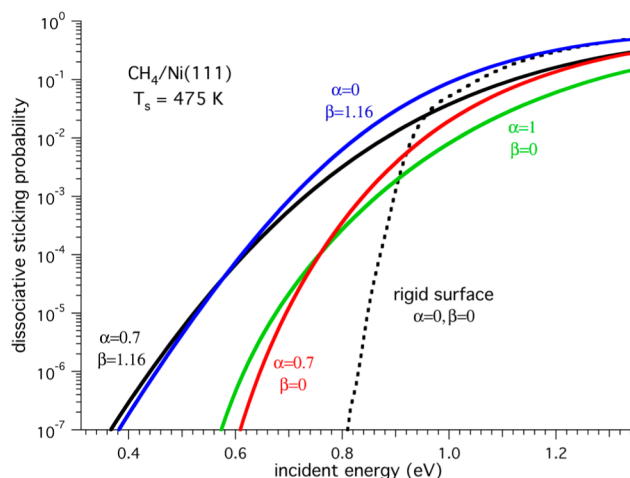


Figure 11. Dissociative sticking probability vs collision energy for methane initially in the ground vibrational state, for five combinations of the phonon coupling parameters, α and β .

The dashed line corresponds to the rigid surface case ($\alpha = \beta = 0$), and at energies below the ZPE-corrected barrier height of 0.94 eV the reactivity decreases rapidly as tunneling

becomes the only reaction mechanism. The SOM corresponds to $\alpha = 1$, $\beta = 0$, and the effects of including this “mechanical” coupling are well-known: the reaction probability at high energies decreases due to lattice recoil, and at low energies the reaction probability increases as larger relative collision velocities are included.^{23,43,79} Note that using the DFT value for α , 0.7, decreases the magnitude of these effects, but not dramatically. On the other hand, the β -term, which describes the modulation of the barrier height with lattice motion, enhances the reactivity at all energies below saturation. For $\beta \approx 1$ eV/Å, a typical value for the surfaces we have studied,⁴² the enhancement of the reactivity at incident energies below the rigid surface barrier height is much larger than for the SOM. Including both terms, and using the DFT values $\alpha = 0.7$ and $\beta = 1.16$ eV/Å, gives a similarly large increase in S_0 , plus some recoil effects at large incident energies.

This enhancement in S_0 below the rigid surface E_a has been referred to as “thermally assisted tunneling”,²³ and because most of the experimental data are at these low energies and the measured S_0 are very small, it has often been assumed that tunneling plays a major role in this reaction. In addition, large isotope effects have been observed in reactions of CH₄ and CD₄ on Ni(111),⁵ Pt(111),²² and other surfaces.⁴³ However, our models suggest that tunneling does not make major contributions to S_0 at typical substrate temperatures.⁷² Although it is difficult to disentangle tunneling from over-the-barrier contributions, we can make a reasonable approximation. In Figure 12 we plot

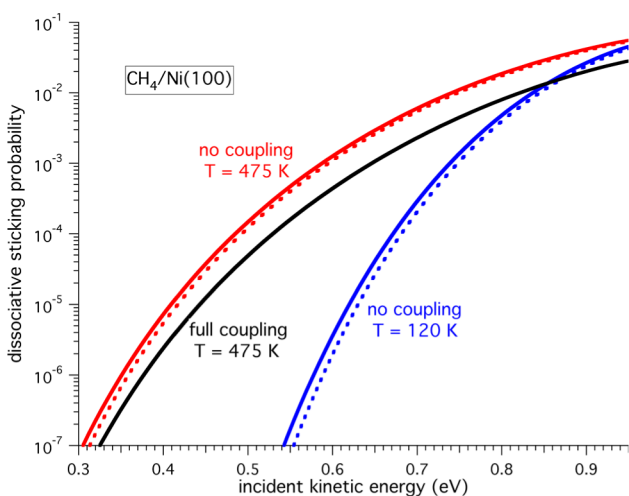


Figure 12. Dissociative sticking probability vs collision energy for methane in the ground vibrational state. The black curve is for full nonadiabatic coupling, and the red and blue curves correspond to zero nonadiabatic coupling. The dashed lines have had the tunneling component removed.

our computed S_0 for CH₄ on Ni(100) at 475 K. We have shown⁷² that if we neglect the Coriolis couplings, $B_{v,v'}$, the ground state S_0 does not change significantly, but if we also set the curvature couplings, $B_{v,15}$, equal to zero, we overestimate the sticking probability a bit, as vibrational excitation no longer competes with reaction. In Figure 12 we plot this vibrationally adiabatic S_0 , and we see that this approximation is not too unreasonable, overestimating the sticking by a factor of 2 to 3. Moreover, because our calculation of P_0 in this limit corresponds to propagation on a single PES, $V_{\text{eff},0}$, we can argue that all probabilities below $P_0 = 0.5$, where the incidence energies are below $E_a = 0.78$ eV, correspond to tunneling. If we simply set P_0 equal to

zero in this tunneling regime, and then average over surface impact sites and the thermal vibrations of the lattice, we get the sticking probabilities plotted as dashed lines in Figure 12. We see that tunneling contributes little for a surface temperature of 475 K, even at energies well below E_a . Thus, the dissociative sticking of methane at 475 K and energies near or below E_a would appear to be dominated by trajectories that collide very near to the top sites of Ni atoms that are near their outer turning points and puckered. At lower incident energies and surface temperatures, tunneling becomes more important. In Figure 12 we plot results for 120 K, and inclusion of tunneling increases S_0 by only a factor of 2 at lower energies.

Ceyer and co-workers⁵ observed that CD₄ was less reactive than CH₄ on Ni(111) at 475 K. In a plot of $\log S_0$ vs E_i , the CD₄ curve was shifted to higher E_i relative to the CH₄ curve by roughly 0.1 eV. We have argued⁷² that part of this is due to the mode softening of Figure 5, which is smaller for CD₄ due to the larger hydrogen mass. Recomputing our RPH for CD₄ on Ni(111), we find that indeed E_a is larger for CD₄ than CH₄ by 0.04 eV. Using this RPH to compute S_0 , we find that in plots of $\log S_0$ vs E_i , the curve for CD₄ is shifted to higher energies relative to the CH₄ curve by roughly 0.06 eV, similar to what has been observed, and at 475 K tunneling is not a major factor.

Several other high-dimensional studies of the dissociative sticking of methane have appeared this past year. Shen et al. used quasiclassical methods to study methane dissociation on moving (111) surfaces of Ni and Pt, using a force field fit to extensive DFT calculations.⁹⁹ This study was able to reproduce the measured S_0 for molecules excited to the $1\nu_3$ state, on both Ni(111) and Pt(111),⁹⁹ at 475 and 150 K, respectively. Moreover, they were able to reproduce the observed difference in reactivity of CH₄ relative to CD₄ on Pt(111),²² without quantum effects, consistent with our arguments in the preceding paragraphs. However, the authors report that the computed S_0 for ground state molecules is too large. This is consistent with a study where we applied quasi-classical methods to our rigid-surface RPH, then used our sudden models to average the resulting P_0 over surface impact sites and lattice motion.¹⁰⁰ The sticking probabilities computed for the excited vibrational states shown in Figures 1 and 8 for Ni(100) and (111), respectively, were in good agreement with both our quantum RPH results and experiment. However, our quasi-classical calculations overestimated the ground state dissociative sticking at energies below the rigid-surface activation energy, when compared with our quantum S_0 . The origin of this behavior was an unphysical flow of ZPE from the nine vibrational modes into the reaction coordinate. We also used this approach to test the perturbative assumptions made in our quantum studies. Calculations were made using both our low-order expansion in b_{ss} (eq 13) and the exact $(1 + b_{ss})^{-2}$ form (eq 9), and our first-order expansion was shown to be accurate at all energies studied, consistent with our quantum studies comparing first- and second-order expansions.

Guo and co-workers fit a 12-DOF PES for methane dissociation on Ni(111) to a very large number of DFT total energy calculations, for the case of a fixed surface impact site (top site) and a rigid surface, and assuming that the surface is flat.⁷⁶ Using this PES, dissociation probabilities were computed quantum mechanically for a reduced 8-DOF model system, after making additional assumptions about the symmetry of the nonreacting methyl group. Surface impact site averaging and thermal lattice effects were then introduced using our sudden models, eqs 2, 4, and 22. The agreement with experiment was very good,

reproducing the vibrational efficacies observed in the experiments,⁷⁶ and adding support to our two sudden models.

Finally, AIMD was used to compute dissociative sticking probabilities for CH_3 incident on $\text{Pt}(111)^{95}$ and $\text{Ni}(111)^{96}$ at high energies, where quantum effects are not expected to be important. The lattice atoms were allowed to move, and the only source of error is the use of classical mechanics and DFT. A detailed analysis of the trajectories allowed us to test some of the dynamical assumptions in our quantum models. First, for ground state molecules with $E_i = 0.78$ eV and $1\nu_3$ molecules with $E_i = 0.51$ eV, reactions on $\text{Pt}(111)$ were shown to occur only for collisions impacting close to the top site,⁹⁵ consistent with our models. In addition, the values for X and Y at the point of surface impact were little changed from their initial values, for both reactive and nonreactive trajectories on both surfaces,^{95,96} consistent with our sudden treatment of these variables. However, the AIMD studies suggest that rotational steering is limited at higher collision energies, and that a sudden treatment might be more reasonable.⁹⁵ To estimate dissociative sticking in the sudden limit, we average our rotationally adiabatic S_0 over all initial angular orientations of the reactive C–H bond, and weigh these using an energy-shifting approximation,⁹⁶ as in eq 22. Our DFT studies show that there is a relatively small variation in energy with respect to the azimuthal orientation of the dissociating C–H bond at the TS.^{41,42} We assume that the PES is uncorrugated in this angle, and the AIMD studies are consistent with this.⁹⁶ ΔV depends most strongly on the polar orientation of the reacting C–H bond, θ . We estimate ΔV by rotating the molecule, at the TS, about $\theta^\dagger = 133^\circ$. For small values of $\Delta\theta = \theta - \theta^\dagger$, eqs 6 and 7 give $\Delta V = 1/2 k_\theta (\Delta\theta)^2$, where $k_\theta = 18.9$ eV/rad². We do not allow the molecule to relax from the TS geometry as we rotate it, and this likely overestimates ΔV . Applying this averaging to the rotationally adiabatic results in Figure 8 leads to the sticking curves in Figure 13. Overall, the effect is to reduce S_0 by roughly a factor of 4.

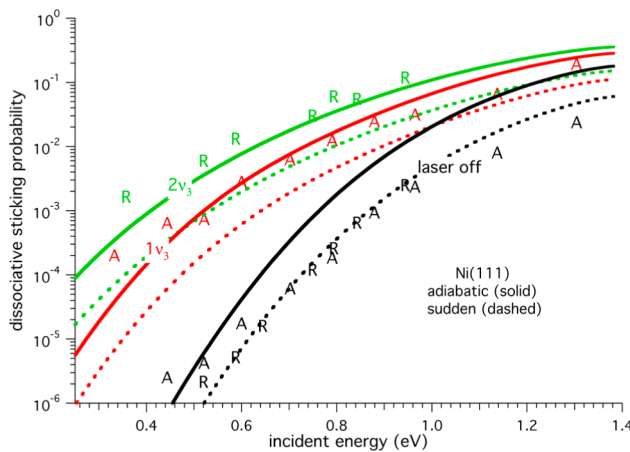


Figure 13. Dissociative sticking probability vs incident energy, for CH_4 dissociation on $\text{Ni}(111)$ at 475 K. Methane is initially in the ground (black), $1\nu_3$ (red), or $2\nu_3$ (green) vibrational state, treating rotational motion in either the adiabatic (solid) or sudden (dashed) limit. Symbols are experimental data from the groups of Utz¹² (A) and Beck (R).²⁰ Reprinted with permission from ref 96 (Figure 8). Copyright 2014 AIP Publishing LLC.

The θ -sudden results for the ground state molecules are now in excellent agreement with experiment. However, it is likely that the θ -sudden limit is too severe and $\Delta V(\theta)$ too large.⁹⁶ It is also likely that our DFT-PBE barrier is too low,⁹⁵ and that these errors cancel

to some extent. The optimal approach is to include θ explicitly in the wave packets of eq 13, though this would complicate a very simple and reasonably accurate model. For now, the curves in Figure 13 provide limiting cases for our model.

V. ADDITIONAL COMMENTS ON MODE-SPECIFIC CHEMISTRY

We have developed a simple model that can reproduce mode-specific behavior, using a relatively small amount of DFT data at the TS and along the MEP. Within our vibrationally adiabatic representation, we have discussed mode-specific behavior, as several authors before us,^{44,59,60,101–103} in terms of mode softening, barriers along vibrationally adiabatic potentials, and transitions between these states due to the nonadiabatic couplings. However, by doing time dependent wave packet dynamics within this representation, we can now quantitatively describe these transitions, and examine how energy moves among the various molecular DOF during a reaction. Moreover, by energy and state resolving these dynamics, relating the asymptotically unbound modes to the translational and rotational behavior of the incident molecule, and adding thermal lattice effects, we can compute sticking probabilities. This allows us to compare directly with state-resolved scattering experiments, and to make quantitative predictions about mode-specific chemistry. Finally, we note that we are not assuming, and indeed do not see, vibrationally adiabatic behavior in these systems. Our choice of representation is by convenience (though it does provide a nice framework from which to examine the dynamics) and convergence with basis size and coupling order is good.

Another characteristic of mode-specific behavior that we observe in our model is that vibrational energy localizes in the reactive bond as the molecule approaches the surface, for vibrational states that strongly promote reaction. Crim and co-workers^{47,103} have observed this in their studies of the gas-phase $\text{CH}_3\text{D} + \text{Cl}$ reaction, and Halonen et al. have noted similar behavior in their model for CH_4 dissociation on Ni.⁶⁰ We represent this two ways in Figure 14. One is to simply use eq 7 to

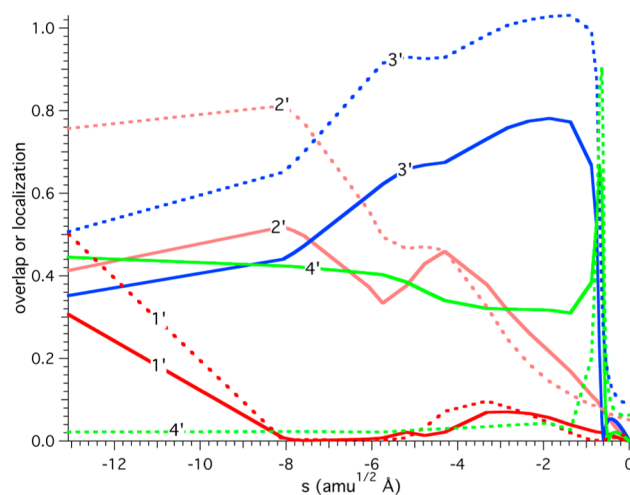


Figure 14. Overlaps (solid lines, eq 24), or bond energy localization (dashed lines), as defined in the text, along the reaction path for CH_4 dissociation on $\text{Ni}(100)$. Results are shown for the 1' (red), 2' (pink), 3' (blue), and 4' (green) modes, using the color scheme and notation of Figure 5.

compute how much a particular bond length changes, δr , when a particular normal coordinate changes by δQ_k . In Figure 14 we plot $|\delta r|/\delta Q_k$ for the reactive C–H bond, for the first four symmetric modes ($\delta Q_k = 0.2 \text{ \AA}$), for $\text{CH}_4/\text{Ni}(100)$. Asymptotically, this ratio is 0.5 for all four bonds, for both the 1' and 3' stretches. However, as the molecule approaches the surface, this vibrational energy completely localizes on the reactive C–H stretch for the 3' mode, whereas the opposite happens for the 1' stretch. For the 2' mode, the vibration is localized on the reactive bond and one other, asymptotically, but $|\delta r|/\delta Q_k$ on the reactive bond goes to zero as the molecule gets close to the TS. This ratio is zero for the 1'' mode and all the other A'' modes, as the reactive C–H stretch is in the plane of symmetry. Overall, this analysis suggests that the ν_1 symmetric stretch (3') should more effectively promote reaction than the ν_3 antisymmetric stretch (1', 2', 1''). The bending modes (e.g., 4') lead to only very small δr , except near the TS (see below).

Perhaps a better measure is to compute how much the motion of the molecule in a particular vibrationally adiabatic state resembles the motion of the molecule as it dissociates at the transition state, because this is not simply a C–H stretch. This is given by

$$\gamma(s) = \sum_{i=1}^{15} L_{i,q}(s) L_{i,F}(0) \quad (24)$$

where again, the “F mode” describes motion of the molecule along the MEP, evaluated here at the TS. For the stretches, the overlaps γ , plotted in Figure 14, closely mirror our results for bond localization, as expected. However, there is a bending component to the dissociation, as seen by the nonzero overlap γ for the 4' bend, and our model suggests a reasonably large η for the 4' mode. Note that as the molecule approaches the avoided crossing near $s \approx -0.6$, the character of the modes changes. In addition, as s goes to zero, γ must go to zero as the modes in eq 24 are then orthogonal to the F mode. The evolution of a molecule initially in the symmetric stretch state (3') can be followed in Figure 5, for the case of large incident energy and/or strong nonadiabatic coupling. As the molecule approaches the surface, the mode distorts so as to become a localized C–H stretch on the reactive bond. At the 3'–4' avoided crossing, the molecule crosses to the 4' state with a high probability. The 4' mode after the crossing is a C–H stretch localized on the reactive bond, as seen in Figure 14. This behavior repeats itself at the 4'–5' and 5'–6' crossings.

It is interesting to compare these ideas with the sudden vector projection (SVP) model developed by Guo and co-workers.¹⁰⁴ In the sudden limit, the reaction is instantaneous and the molecule does not have time to change its internal state. Quantum mechanically, S_0 would then be approximately proportional to the square of a Franck–Condon factor, the overlap of the initial vibrational wave function with that of the molecule at the TS. In the SVP model the Franck–Condon factor is approximated by eq 24, where s corresponds to the molecule far above the surface. It is important to maximize this overlap by making the molecular alignment at s similar to that at the TS.^{76,104} Our AIMD studies lend some support to the SVP model, as the rotational dynamics appear more sudden than adiabatic. In the rotationally sudden limit the incident molecule at s has the same angular orientation as at the TS, and as noted, eq 24 describes how much the molecular motion for mode q resembles the motion of the molecule as it dissociates.

Table 2. Experimental Efficacies (η) and Computed Normal Mode Overlaps (γ)

	Ni(111)		Ni(100)		Pt(111)		Pt(110)-(1x2)	
	η	γ	η	γ	η	γ	η	γ
$1\nu_1$		0.40	1.4^{14}	0.31		0.37		0.39
$1\nu_3$	1.25 ¹²	0.35	0.94^8	0.26	0.7 ³¹	0.41		0.29
$1\nu_4$		0.16		0.16		0.16		0.13
T_z^{α}		0.22		0.26		0.29		0.29
T_x		0.00		0.13		0.00		0.00
T_y		0.05		0.13		0.00		0.00

^aThe T_i are overlaps with vectors describing center-of-mass translation in the $i = X, Y, Z$ directions. Adapted from ref 96.

In Table 2 we list the SVP γ for the dissociative adsorption of CH_4 on four surfaces. To compute $L_{i,q}(s)$ in eq 24, we start with the TS geometry of CH_4 , remove the entire metal slab, and relax the molecule (roughly preserving the TS orientation), and then we compute the molecule's normal modes. This is similar to the procedure used by Guo and co-workers in their study on Ni(111), where they report overlaps of 0.40, 0.31, and 0.20 for the ν_1 , ν_3 , and ν_4 states,⁷⁶ similar to our values. As in that work, for degenerate vibrations we average the overlaps of the components. For Ni(100) we see that the overlap γ is larger for the $1\nu_1$ state than for the $1\nu_3$ state, consistent with the results in Figure 1 and the experimental efficacies η . We also compute overlaps with translation, where L_q in eq 24 is replaced by the vector describing translation of the molecule in the X , Y , and Z directions. The SVP overlaps suggest that on Ni(100) the symmetric stretch is more effective at promoting dissociation than normal translational energy, whereas the antisymmetric stretch is similar to translation, consistent with efficacies larger than and close to 1, respectively. The overlap γ for the $1\nu_3$ stretch is also larger than the Z -overlap on both Ni(111) and Pt(111), though for the former $\eta > 1$ and the latter $\eta < 1$. We find that the SVP consistently predicts that the bending vibrations should have smaller efficacies for promoting dissociation than the stretches. Though no data exist for the $1\nu_4$ state, an experimental study of CH_4 excited to the $3\nu_4$ state reacting on Ni(111) and Ni(100) reports $\eta = 0.72$ and $\eta \leq 0.5$, respectively,¹³ consistent with this. Comparing across metals for the $1\nu_3$ state, we see that, although the measured efficacies scale with the γ on the Ni surfaces, Pt(111) has the largest overlap but the smallest η .

For translation of the molecule normal to the surface, along Z , the overlap is relatively large, but less than 1 for this late barrier system. For Ni(111) and Pt(111), the overlaps with motion parallel to the surface (X , Y) are small, which is consistent with experiments that find normal energy scaling on these metals.^{5,22} However, on Ni(100) we find non-negligible overlaps for parallel motion. Our γ suggest that increased parallel kinetic energy would increase S_0 , but that the overall behavior is closer to normal rather than total energy scaling, and this is what has been observed experimentally.⁶

VI. CONCLUSIONS

We have characterized the transition states for methane dissociation on several Ni and Pt surfaces with a focus on how they are modified by lattice motion. The molecule–phonon coupling is found to be unusually strong; not only does the location of the TS change with lattice motion, but also the height of the barrier to dissociation changes dramatically. Quantum scattering calculations incorporating this coupling show that

including lattice motion can change S_0 by several orders of magnitude. In fact, a reasonable comparison with experiment cannot be made without inclusion of these effects.

How general is this behavior? For the direct dissociative sticking of H₂, perhaps the most-studied reaction in surface science, temperature effects are relatively minor. This is partly due to the small molecule-to-metal mass ratio (weak “mechanical” coupling) and the fact that lattice relaxation for H adsorption is minor (small β). However, recent theoretical studies have explored some of the T effects seen in H₂/Cu scattering^{105,106} and have also characterized the phonon coupling in terms of α and β .¹⁰⁷ In addition, the effects of thermal expansion on scattering have recently been explored and found to be important.¹⁰⁶ More generally, the mechanical effects described by the SOM and SMM, with the proper α , should be important for heavier molecules and/or larger E_i . The unusually large coupling of particular interest here, $\beta \neq 0$, should occur whenever there is lattice relaxation in the presence of the dissociating and adsorbing molecule. Although there is typically much lattice rearrangement for chemisorption on C and Si substrates, this is not always the case on metals. However, recent theoretical work has found that there can be a rather complicated lattice relaxation when H₂O dissociatively chemisorbs on Ni surfaces, and the temperature effects are found to be strong,^{108,109} though weaker than for methane. It is likely that other molecules of interest will exhibit similar behavior.

We have developed simple models that incorporate these lattice effects into rigid-substrate calculations. We have also developed a sudden treatment of motion of the methane parallel to the surface, effectively averaging over surface impact sites. These approximations have been shown to be both reasonable and accurate. Moreover, all of the parameters in these models can be computed via first-principles, from properties of the TS. Approximations such as these are essential in quantum descriptions of reactive scattering of polyatomic and heavy diatomic molecules, as both M and M_s are much larger than 1, and treating Q, X, and Y explicitly in a quantum calculation is prohibitive. These approximations have recently been used by other groups, in high-dimensional quantum studies of methane and water dissociation.^{76,108,109} We have also shown that the PES is relatively insensitive to the azimuthal orientation of the dissociating bond, and this “flat surface” approximation has also been used in recent quantum studies.^{76,110–112}

We have developed a quantum reactive scattering approach based on the reaction path Hamiltonian that allows us to include all of the methane DOFs, and lattice effects, given our sudden treatments of X, Y, and Q. Agreement with experiment with respect to variation of S_0 with collision energy, substrate temperature, and molecular vibrational state is good. More importantly, we have a relatively simple and realistic model that includes all DOFs and allows us to explore the dynamics of energy flow during a reactive collision. All potentials and parameters defining our equations of motion can be derived from first principles. In addition to helping better elucidate the effects of lattice motion by allowing for a direct comparison with experimental data, we have gained some insight into mode-specific chemistry. Within the framework of a vibrationally adiabatic basis, we have been able to explain our results in terms of mode softening and vibrationally adiabatic barriers, symmetry, and nonadiabatic transitions. We do not mean to suggest that this reaction is vibrationally adiabatic. In fact, we are likely closer to the opposite limit; the nonadiabatic couplings are strong and necessary to explain the dynamics. However, our choice for this basis makes our approach tractable, and results converge rapidly with basis size. Applying the SVP model to our systems, we see some correlation with experimentally measured efficacies.

In general, stretches have a larger overlap with motion at the TS than bends, and thus larger efficacies for promoting reaction. We have also been able to relate this approach to localization of energy in the reactive bond. Finally, we have extended the SVP model to include motion parallel and perpendicular to the metal surface, and get results in excellent agreement with experiments on Ni(111), Ni(100), and Pt(111). How general is mode-specific chemistry for reactions on metals? A recent study of the dissociative chemisorption of water on Ni(111) finds strong vibrational promotion of S_0 , and theory suggests mode-specific behavior.¹⁰⁹ Recent arguments by Killelea and Utz suggest this behavior might be more common than expected.¹¹³

Finally, our approach has proven capable of describing, quantum mechanically, the reaction dynamics of a polyatomic molecule in the presence of a bath. Once the potentials, frequencies, and couplings have been computed via DFT, the actual scattering calculation requires only seconds to minutes on a single processor. We note that, although we have shown that tunneling is not important at higher T, and classical mechanics appears to work well at high E_i or for vibrationally excited states, our quantum method is still preferable. It keeps the ZPE under control, is better at low E_i , and for ground state molecules, providing a consistent treatment at all energies, includes tunneling when important, and it is easier to do; far fewer DFT energies are required to construct the PES, we do not need to average over a great many trajectories, and we can go to very small S_0 , where intractable numbers of classical trajectories might be required for decent statistics. In the future we will likely introduce a better treatment of θ , either using traditional methods to include it in the wavepackets or including the asymptotically unbound modes directly in our basis set. Addition of more DOF is straightforward, and treating lattice motion directly in this manner is under consideration. Finally, it is possible that these methods can be used to explore the reactions of polyatomic molecules in the gas phase. Reactions of methane with halogens is an obvious place to start.

■ AUTHOR INFORMATION

Corresponding Author

*B. Jackson. E-mail: jackson@chem.umass.edu.

Notes

The authors declare no competing financial interest.

Biographies

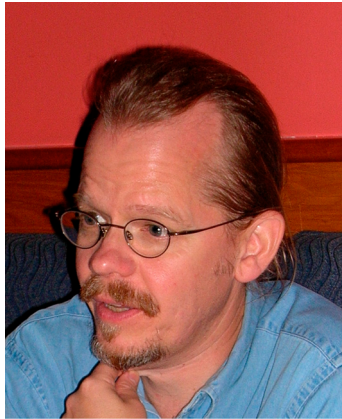


Sven Nave completed his Ph.D. in 2004 at the Université des Sciences et Technologies de Lille, France, under the supervision of Dr. Didier Lemoine. From 2005 to 2009 Dr. Nave was a postdoctoral researcher at the University of Massachusetts, Amherst, working with Professor Bret Jackson.

In 2010, Dr. Nave was also a postdoctoral researcher at the Université Paul Sabatier, France. He is now an associate professor at the Université Paris-Sud Orsay, France, working on various projects related to quantum molecular dynamics on surfaces.



Ashwani K. Tiwari received his Ph.D. in theoretical chemistry working under the supervision of Prof. N. Sathyamurthy at the Indian Institute of Technology, Kanpur, in 2007. During the period May 2007–April 2008, he was a postdoctoral fellow with Prof. Niels E. Henriksen at the Technical University of Denmark. From May 2008 to April 2010, he was a postdoctoral fellow with Prof. Bret Jackson at the University of Massachusetts, Amherst. Currently, he is an Assistant Professor at the Indian Institute of Science Education and Research, Kolkata. His research interests involve the dynamics of laser–molecule and molecule–metal surface interactions.



Bret Jackson received his B.S. degree from Carnegie Mellon University in 1979 and his Ph.D. from the Massachusetts Institute of Technology in 1983, both in chemistry. From 1983 to 1985 he was a Postdoctoral Associate at the University of California, working with Prof. Horia Metiu. He has been a Professor in the Chemistry Department at the University of Massachusetts, Amherst, since 1985, where his research has focused on exploring the dynamics of various molecule–surface interactions.

ACKNOWLEDGMENTS

B. Jackson gratefully acknowledges support from the Division of Chemical Sciences, Office of Basic Energy Sciences, Office of Energy Research, U.S. Department of Energy, under Grant DE-FG02-87ER13744.

REFERENCES

- (1) Larsen, J. H.; Chorkendorff, I. From Fundamental Studies of Reactivity on Single Crystals to the Design of Catalysts. *Surf. Sci. Rep.* **1999**, *35*, 163–222.
- (2) Juurlink, L. B. F.; Killelea, D. R.; Utz, A. L. State-Resolved Probes of Methane Dissociation Dynamics. *Prog. Surf. Sci.* **2009**, *84*, 69–134.
- (3) Utz, A. L. Mode Selective Chemistry at Surfaces. *Curr. Opin. Solid State Mater. Sci.* **2009**, *13*, 4–12.
- (4) Beck, R. D.; Utz, A. L. Quantum-State Resolved Gas/Surface Reaction Dynamics Experiments. In *Dynamics of Gas-Surface Interactions*; Muiño, R. D., Busnengo, H. F., Eds.; Springer Series in Surface Sciences; Springer-Verlag: Berlin, Heidelberg, 2013; Vol. 50, pp 179–212.
- (5) Lee, M. B.; Yang, Q. Y.; Ceyer, S. T. Dynamics of the Activated Dissociative Chemisorption of CH_4 and Implication for the Pressure Gap in Catalysis - a Molecular-Beam High-Resolution Electron-Energy Loss Study. *J. Chem. Phys.* **1987**, *87*, 2724–2741.
- (6) Holmlund, P. M.; Wambach, J.; Chorkendorff, I. Molecular Beam Study of Dissociative Sticking on $\text{Ni}(100)$. *J. Chem. Phys.* **1995**, *102*, 8255–8263.
- (7) Holmlund, P. M.; Larsen, J. H.; Chorkendorff, I. Modification of $\text{Ni}(111)$ Reactivity toward CH_4 , CO, and D-2 by Two-Dimensional Alloying. *J. Chem. Phys.* **1996**, *104*, 7289–7295.
- (8) Juurlink, L. B. F.; McCabe, P. R.; Smith, R. R.; DiCologero, C. L.; Utz, A. L. Eigenstate-Resolved Studies of Gas-Surface Reactivity: $\text{CH}_4(\nu_3)$ Dissociation on $\text{Ni}(100)$. *Phys. Rev. Lett.* **1999**, *83*, 868–871.
- (9) Egeberg, R. C.; Ullmann, S.; Alstrup, I.; Mullins, C. B.; Chorkendorff, I. Dissociation of CH_4 on $\text{Ni}(111)$ and $\text{Ru}(0001)$. *Surf. Sci.* **2002**, *497*, 183–193.
- (10) Schmid, M. P.; Maroni, P.; Beck, R. D.; Rizzo, T. R. Surface Reactivity of Highly vibrationally Excited Molecules Prepared by Pulsed Laser Excitation: $\text{CH}_4(2\nu_3)$ on $\text{Ni}(100)$. *J. Chem. Phys.* **2002**, *117*, 8603.
- (11) Beck, R. D.; Maroni, P.; Papageorgopoulos, D. C.; Dang, T. T.; Schmid, M. P.; Rizzo, T. R. Vibrational Mode-Specific Reaction of Methane on a Nickel Surface. *Science* **2003**, *302*, 98–100.
- (12) Smith, R. R.; Killelea, D. R.; DelSesto, D. F.; Utz, A. L. Preference for Vibrational over Translational Energy in a Gas-Surface Reaction. *Science* **2004**, *304*, 992–995.
- (13) Juurlink, L. B. F.; Smith, R. R.; Killelea, D. R.; Utz, A. L. Comparative Study of C-H Stretch and Bend Vibrations in Methane Activation on $\text{Ni}(100)$ and $\text{Ni}(111)$. *Phys. Rev. Lett.* **2005**, *94*, 208303.
- (14) Maroni, P.; Papageorgopoulos, D. C.; Sacchi, M.; Dang, T. T.; Beck, R. D.; Rizzo, T. R. State-Resolved Gas-Surface Reactivity of Methane in the Symmetric C-H Stretch Vibration on $\text{Ni}(100)$. *Phys. Rev. Lett.* **2005**, *94*, 246104.
- (15) Killelea, D. R.; Campbell, V. L.; Shuman, N. S.; Utz, A. L. Bond-Selective Control of a Heterogeneously Catalyzed Reaction. *Science* **2008**, *319*, 790–793.
- (16) Killelea, D. R.; Campbell, V. L.; Shuman, N. S.; Smith, R. R.; Utz, A. L. Surface Temperature Dependence of Methane Activation on $\text{Ni}(111)$. *J. Phys. Chem. C* **2009**, *113*, 20618–20622.
- (17) Yoder, B. L.; Bisson, R.; Beck, R. D. Steric Effects in the Chemisorption of vibrationally Excited Methane on $\text{Ni}(100)$. *Science* **2010**, *329*, 553–556.
- (18) Yoder, B. L.; Bisson, R.; Morten Hundt, P.; Beck, R. D. Alignment Dependent Chemisorption of vibrationally Excited $\text{CH}_4(\nu_3)$ on $\text{Ni}(100)$, $\text{Ni}(110)$, and $\text{Ni}(111)$. *J. Chem. Phys.* **2011**, *135*, 224703.
- (19) Chen, N.; Huang, Y. L.; Utz, A. L. State-Resolved Reactivity of Methane ($\nu(2) + \nu(4)$) on $\text{Ni}(111)$. *J. Phys. Chem. A* **2013**, *117*, 6250–6255.
- (20) Bisson, R.; Sacchi, M.; Dang, T. T.; Yoder, B.; Maroni, P.; Beck, R. D. State-Resolved Reactivity of $\text{CH}_4(2\nu(3))$ on $\text{Pt}(111)$ and $\text{Ni}(111)$: Effects of Barrier Height and Transition State Location. *J. Phys. Chem. A* **2007**, *111*, 12679–12683.
- (21) Schoofs, G. R.; Arumainayagam, C. R.; McMaster, M. C.; Madix, R. J. Dissociative Chemisorption of Methane on $\text{Pt}(111)$. *Surf. Sci.* **1989**, *215*, 1–28.
- (22) Luntz, A. C.; Bethune, D. S. Activation of Methane Dissociation on a $\text{Pt}(111)$ Surface. *J. Chem. Phys.* **1989**, *90*, 1274–1280.
- (23) Harris, J.; Simon, J.; Luntz, A. C.; Mullins, C. B.; Rettner, C. T. Thermally Assisted Tunneling: CH_4 Dissociation on $\text{Pt}(111)$. *Phys. Rev. Lett.* **1991**, *67*, 652–655.

- (24) Oakes, D. J.; Mccoustra, M. R. S.; Chesters, M. A. Dissociative Adsorption of Methane on Pt(111) Induced by Hyperthermal Collisions. *Faraday Discuss.* **1993**, *96*, 325–336.
- (25) Walker, A. V.; King, D. A. Dynamics of the Dissociative Adsorption of Methane on Pt{110}(1×2). *Phys. Rev. Lett.* **1999**, *82*, 5156–5159.
- (26) Walker, A. V.; King, D. A. Dynamics of Dissociative Methane Adsorption on Metals: CH₄ on Pt{110}(1×2). *J. Chem. Phys.* **2000**, *112*, 4739–4748.
- (27) Higgins, J.; Conjusteau, A.; Scoles, G.; Bernasek, S. L. State Selective Vibrational (2ν(3)) Activation of the Chemisorption of Methane on Pt(111). *J. Chem. Phys.* **2001**, *114*, 5277–5283.
- (28) Bisson, R.; Sacchi, M.; Beck, R. D. State-Resolved Reactivity of CH₄ on Pt(110)-(1×2): The Role of Surface Orientation and Impact Site. *J. Chem. Phys.* **2010**, *132*, 094702.
- (29) Bisson, R.; Sacchi, M.; Beck, R. D. Mode-Specific Reactivity of CH₄ on Pt(110)-(1×2): The Concerted Role of Stretch and Bend Excitation. *Phys. Rev. B* **2010**, *82*, 121404.
- (30) Chen, L.; Ueta, H.; Bisson, R.; Beck, R. D. vibrationally Bond-Selected Chemisorption of Methane Isotopologues on Pt(111) Studied by Reflection Absorption Infrared Spectroscopy. *Faraday Discuss.* **2012**, *157*, 285–295.
- (31) Ueta, H.; Chen, L.; Beck, R. D.; Colon-Diaz, I.; Jackson, B. Quantum State-Resolved CH₄ Dissociation on Pt(111): Coverage Dependent Barrier Heights from Experiment and Density Functional Theory. *Phys. Chem. Chem. Phys.* **2013**, *15*, 20526–20535.
- (32) McMaster, M. C.; Madix, R. J. Alkane Dissociation Dynamics on Pt(110)-(1×2). *J. Chem. Phys.* **1993**, *98*, 9963–9976.
- (33) Yang, H.; Whitten, J. L. Dissociative Chemisorption of CH₄ on Ni(111). *J. Chem. Phys.* **1992**, *96*, 5529–5537.
- (34) Kratzer, P.; Hammer, B.; Norskov, J. K. A Theoretical Study of CH₄ Dissociation on Pure and Gold-Alloyed Ni(111) Surfaces. *J. Chem. Phys.* **1996**, *105*, 5595–5604.
- (35) Watwe, R. M.; Bengaard, H. S.; Rostrup-Nielsen, J. R.; Dumesic, J. A.; Norskov, J. K. Theoretical Studies of Stability and Reactivity of CH_x Species on Ni(111). *J. Catal.* **2000**, *189*, 16–30.
- (36) Bengaard, H. S.; Norskov, J. K.; Sehested, J.; Clausen, B. S.; Nielsen, L. P.; Molenbroek, A. M.; Rostrup-Nielsen, J. R. Steam Reforming and Graphite Formation on Ni Catalysts. *J. Catal.* **2002**, *209*, 365–384.
- (37) Abild-Pedersen, F.; Lytken, O.; Engbaek, J.; Nielsen, G.; Chorkendorff, I.; Norskov, J. K. Methane Activation on Ni(111): Effects of Poisons and Step Defects. *Surf. Sci.* **2005**, *590*, 127–137.
- (38) Henkelman, G.; Arnaldsson, A.; Jónsson, H. Theoretical Calculations of CH₄ and H₂ Associative Desorption from Ni(111): Could Subsurface Hydrogen Play an Important Role? *J. Chem. Phys.* **2006**, *124*, 044706.
- (39) Nave, S.; Jackson, B. Methane Dissociation on Ni(111): The Role of Lattice Reconstruction. *Phys. Rev. Lett.* **2007**, *98*, 173003.
- (40) Nave, S.; Jackson, B. Methane dissociation on Ni(111): The Effects of Lattice Motion and Relaxation on Reactivity. *J. Chem. Phys.* **2007**, *127*, 224702.
- (41) Nave, S.; Jackson, B. Methane Dissociation on Ni(111) And Pt(111): Energetic and Dynamical Studies. *J. Chem. Phys.* **2009**, *130*, 054701.
- (42) Nave, S.; Tiwari, A. K.; Jackson, B. Methane Dissociation and Adsorption on Ni(111), Pt(111), Ni(100), Pt(100), and Pt(110)-(1×2): Energetic Study. *J. Chem. Phys.* **2010**, *132*, 054705.
- (43) Luntz, A. C.; Harris, J. CH₄ Dissociation on Metals - a Quantum Dynamics Model. *Surf. Sci.* **1991**, *258*, 397–426.
- (44) Corchado, J. C.; Truhlar, D. G.; Espinosa-Garcia, J. Potential Energy Surface, Thermal, And State-Selected Rate Coefficients, And Kinetic Isotope Effects for Cl+CH₄ → HCl+CH₃. *J. Chem. Phys.* **2000**, *112*, 9375–9389.
- (45) Crim, F. F. Chemical Dynamics of vibrationally Excited Molecules: Controlling Reactions in Gases and on Surfaces. *Proc. Natl. Acad. Sci. U. S. A.* **2008**, *105*, 12654–12661.
- (46) Kim, Z. H.; Bechtel, H. A.; Zare, R. N. Vibrational Control in the Reaction of Methane with Atomic Chlorine. *J. Am. Chem. Soc.* **2001**, *123*, 12714–12715.
- (47) Yoon, S.; Holiday, R. J.; Crim, F. F. vibrationally Controlled Chemistry: Mode- And Bond-Selected Reaction of CH₃D with Cl. *J. Phys. Chem. B* **2005**, *109*, 8388–8392.
- (48) Czako, G.; Bowman, J. M. Dynamics of the Reaction of Methane with Chlorine Atom on an Accurate Potential Energy Surface. *Science* **2011**, *334*, 343–346.
- (49) Carré, M. N.; Jackson, B. Dissociative chemisorption of CH(4) on Ni: The role of molecular orientation. *J. Chem. Phys.* **1998**, *108*, 3722–3730.
- (50) Xiang, Y.; Zhang, J. Z. H.; Wang, D. Y. Semirigid Vibrating Rotor Target Model for CH₄ Dissociation on a Ni(111) Surface. *J. Chem. Phys.* **2002**, *117*, 7698.
- (51) Xiang, Y.; Zhang, J. Z. H. A Mixed Quantum-Classical Semirigid Vibrating Rotor Target Approach to Methane Dissociation on Ni Surface. *J. Chem. Phys.* **2003**, *118*, 8954.
- (52) Tiwari, A. K.; Nave, S.; Jackson, B. Methane Dissociation on Ni(111): A New Understanding of the Lattice Effect. *Phys. Rev. Lett.* **2009**, *103*, 253201.
- (53) Nave, S.; Jackson, B. Vibrational Mode-Selective Chemistry: Methane Dissociation on Ni(100). *Phys. Rev. B* **2010**, *81*, 233408.
- (54) Tiwari, A. K.; Nave, S.; Jackson, B. The Temperature Dependence of Methane Dissociation on Ni(111) And Pt(111): Mixed Quantum-Classical Studies of the Lattice Response. *J. Chem. Phys.* **2010**, *132*, 134702.
- (55) Teixidor, M. M.; Huarte-Larranaga, F. Methane Dissociation on Ni(111): Reaction Probabilities Using Direct and Initial State Selected Approaches. *Chem. Phys.* **2012**, *399*, 264–271.
- (56) Jansen, A. P. J.; Burghgraef, H. MCTDH Study of CH₄ Dissociation on Ni(111). *Surf. Sci.* **1995**, *344*, 149–158.
- (57) Milot, R.; Jansen, A. P. J. Bond Breaking in vibrationally Excited Methane on Transition-Metal Catalysts. *Phys. Rev. B* **2000**, *61*, 15657–15660.
- (58) Krishnamohan, G. P.; Olsen, R. A.; Kroes, G. J.; Gatti, F.; Woittequand, S. Quantum Dynamics of Dissociative Chemisorption of CH₄ on Ni(111): Influence of the Bending Vibration. *J. Chem. Phys.* **2010**, *133*, 144308.
- (59) Prasanna, K. G.; Olsen, R. A.; Valdes, A.; Kroes, G. J. Towards an Understanding of the Vibrational Mode Specificity for Dissociative Chemisorption of CH₄ On Ni(111): a 15 Dimensional Study. *Phys. Chem. Chem. Phys.* **2010**, *12*, 7654–7661.
- (60) Halonen, L.; Bernasek, S. L.; Nesbitt, D. J. Reactivity of vibrationally Excited Methane on Nickel Surfaces. *J. Chem. Phys.* **2001**, *115*, 5611–5619.
- (61) Abbott, H. L.; Bukoski, A.; Harrison, I. Microcanonical Unimolecular Rate Theory at Surfaces. II. Vibrational State Resolved Dissociative Chemisorption of Methane on Ni(100). *J. Chem. Phys.* **2004**, *121*, 3792–3810.
- (62) Bukoski, A.; Harrison, I. Assessing a Microcanonical Theory of Gas-Surface Reactivity: Applicability to Thermal Equilibrium, Non-equilibrium, And Eigenstate-Resolved Dissociation of Methane on Ni(100). *J. Chem. Phys.* **2003**, *118*, 9762–9768.
- (63) Ukrainstev, V. A.; Harrison, I. A Statistical-Model for Activated Dissociative Adsorption - Application to Methane Dissociation on Pt(111). *J. Chem. Phys.* **1994**, *101*, 1564–1581.
- (64) Kresse, G.; Hafner, J. Ab Initio Molecular-Dynamics for Liquid-Metals. *Phys. Rev. B* **1993**, *47*, 558–561.
- (65) Kresse, G.; Hafner, J. Ab-Initio Molecular-Dynamics Simulation of the Liquid-Metal Amorphous-Semiconductor Transition in Germanium. *Phys. Rev. B* **1994**, *49*, 14251–14269.
- (66) Kresse, G.; Furthmuller, J. Efficient Iterative Schemes for Ab Initio Total-Energy Calculations Using a Plane-Wave Basis Set. *Phys. Rev. B* **1996**, *54*, 11169–11186.
- (67) Kresse, G.; Furthmuller, J. Efficiency of Ab-Initio Total Energy Calculations for Metals and Semiconductors Using a Plane-Wave Basis Set. *J. Comput. Mater. Sci.* **1996**, *6*, 15–50.

- (68) Kresse, G.; Joubert, D. From Ultrasoft Pseudopotentials to the Projector Augmented-Wave Method. *Phys. Rev. B* **1999**, *59*, 1758–1775.
- (69) Blöchl, P. E. Projector Augmented-Wave Method. *Phys. Rev. B* **1994**, *50*, 17953–17979.
- (70) Perdew, J. P.; Burke, K.; Ernzerhof, M. Generalized Gradient Approximation Made Simple. *Phys. Rev. Lett.* **1996**, *77*, 3865–3868.
- (71) Perdew, J. P.; Burke, K.; Ernzerhof, M. Generalized Gradient Approximation Made Simple (vol 77, pg 3865, 1996). *Phys. Rev. Lett.* **1997**, *78*, 1396–1396.
- (72) Jackson, B.; Nave, S. The Dissociative Chemisorption of Methane on Ni(100): Reaction Path Description of Mode-Selective Chemistry. *J. Chem. Phys.* **2011**, *135*, 114701.
- (73) Han, D.; Nave, S.; Jackson, B. The Dissociative Chemisorption of Methane on Pt(110)-(1×2): The Effects of Lattice Motion on Reactions at Step Edges. *J. Phys. Chem. A* **2013**, *117*, 8651–8659.
- (74) Henkelman, G.; Ubaruaga, B. P.; Jónsson, H. A Climbing Image Nudged Elastic Band Method for Finding Saddle Points and Minimum Energy Paths. *J. Chem. Phys.* **2000**, *113*, 9901–9904.
- (75) Henkelman, G.; Jónsson, H. Improved Tangent Estimate in the Nudged Elastic Band Method for Finding Minimum Energy Paths and Saddle Points. *J. Chem. Phys.* **2000**, *113*, 9978–9985.
- (76) Jiang, B.; Liu, R.; Li, J.; Xie, D. Q.; Yang, M. H.; Guo, H. Mode Selectivity in Methane Dissociative Chemisorption on Ni(111). *Chem. Sci.* **2013**, *4*, 3249–3254.
- (77) Anghel, A.; Wales, D.; Jenkins, S.; King, D. Pathways for Dissociative Methane Chemisorption on Pt{110}-(1×2). *Phys. Rev. B* **2005**, *71*, 113410.
- (78) Henkelman, G.; Jónsson, H. Theoretical Calculations of Dissociative Adsorption of CH₄ on an Ir(111) Surface. *Phys. Rev. Lett.* **2001**, *86*, 664–667.
- (79) Hand, M.; Harris, J. Recoil Effects in Surface Dissociation. *J. Chem. Phys.* **1990**, *92*, 7610–7617.
- (80) Marcus, R. A. On Analytical Mechanics of Chemical Reactions. Quantum Mechanics of Linear Collisions. *J. Chem. Phys.* **1966**, *45*, 4493.
- (81) Miller, W. H.; Handy, N. C.; Adams, J. E. Reaction-Path Hamiltonian for Polyatomic-Molecules. *J. Chem. Phys.* **1980**, *72*, 99–112.
- (82) Lu, D. H.; Truong, T. N.; Melissas, V. S.; Lynch, G. C.; Liu, Y. P.; Garrett, B. C.; Steckler, R.; Isaacson, A. D.; Rai, S. N.; Hancock, G. C.; Lauderdale, J. G.; Joseph, T.; Truhlar, D. G. Polyrate-4 - a New Version of a Computer-Program for the Calculation of Chemical-Reaction Rates for Polyatomics. *Comput. Phys. Commun.* **1992**, *71*, 235–262.
- (83) Miller, W. H.; Shi, S. Unified Semi-Classical Perturbation and Infinite-Order Sudden Approximation, with Application to the Reaction-Path Hamiltonian Model. *J. Chem. Phys.* **1981**, *75*, 2258–2264.
- (84) Miller, W. H.; Schwartz, S. System-Bath Decomposition of the Reaction-Path Hamiltonian for Polyatomic Scattering - Quantum Perturbative Treatment. *J. Chem. Phys.* **1982**, *77*, 2378–2382.
- (85) Cerjan, C. J.; Shi, S.; Miller, W. H. Applications of a Simple Dynamical Model to the Reaction-Path Hamiltonian - Tunneling Corrections to Rate Constants, Product State Distributions, Line Widths of Local Mode Overtones, and Mode Specificity in Unimolecular Decomposition. *J. Phys. Chem.* **1982**, *86*, 2244–2251.
- (86) Miller, W. H. Reaction-Path Dynamics for Polyatomic Systems. *J. Phys. Chem.* **1983**, *87*, 3811–3819.
- (87) Fang, J. Y.; Hammes-Schiffer, S. Time-Dependent Self-Consistent-Field Dynamics Based on a Reaction Path Hamiltonian. I. Theory. *J. Chem. Phys.* **1998**, *108*, 7085–7099.
- (88) Billing, G. D. Application of the Reaction Path Method to the Reaction: H+CH₄ → H₂+CH₃. *Chem. Phys.* **2002**, *277*, 325–340.
- (89) Stopera, C. J.; Bladow, L. L.; Thweatt, W. D.; Page, M. Mixed Quantum-Classical Reaction Path Dynamics of C₂H₅F → C₂H₄ + HF. *J. Phys. Chem. A* **2008**, *112*, 11931–11941.
- (90) Juurlink, L. B. F.; Smith, R. R.; Utz, A. L. The Role of Rotational Excitation in the Activated Dissociative Chemisorption of vibrationally Excited Methane on Ni(100). *Faraday Discuss.* **2000**, *117*, 147–160.
- (91) Jackson, B.; Nave, S. The Dissociative Chemisorption of Methane on Ni(111): The effects of Molecular Vibration and Lattice Motion. *J. Chem. Phys.* **2013**, *138*, 174705.
- (92) Dai, J. Q.; Zhang, J. Z. H. Time-Dependent Wave Packet Approach to State-to-State Reactive Scattering and Application to H+O₂ Reaction. *J. Phys. Chem.* **1996**, *100*, 6898–6903.
- (93) Zhang, D. H.; Wu, Q.; Zhang, J. Z. H. A Time-Dependent Approach to Flux Calculation in Molecular Photofragmentation - Vibrational Predissociation of HF-DF. *J. Chem. Phys.* **1995**, *102*, 124–132.
- (94) Diaz, C.; Pijper, E.; Olsen, R. A.; Busnengo, H. F.; Auerbach, D. J.; Kroes, G. J. Chemically Accurate Simulation of a Prototypical Surface Reaction: H₂ Dissociation on Cu(111). *Science* **2009**, *326*, 832–834.
- (95) Nattino, F.; Ueta, H.; Chadwick, H.; van Reijzen, M. E.; Beck, R. D.; Jackson, B.; van Hemert, M. C.; Kroes, G. J. Ab Initio Molecular Dynamics Calculations versus Quantum State-Resolved Experiments on CHD₃ + Pt(111): New Insights into a Prototypical Gas-Surface Reaction. *J. Phys. Chem. Lett.* **2014**, *5*, 1294–1299.
- (96) Jackson, B.; Nattino, F.; Kroes, G. J. Dissociative Chemisorption of Methane on Metal Surfaces: Tests of Dynamical Assumptions Using Quantum Models and Ab Initio Molecular Dynamics. *J. Chem. Phys.* **2014**, *141*, 054102.
- (97) Sacchi, M.; Wales, D. J.; Jenkins, S. J. Mode-Specific Chemisorption of CH₄ on Pt{110}-(1×2) Explored by First-Principles Molecular Dynamics. *J. Phys. Chem. C* **2011**, *115*, 21832–21842.
- (98) Sacchi, M.; Wales, D. J.; Jenkins, S. J. Bond-Selective Energy Redistribution in the Chemisorption of CH₃D and CD₃H on Pt{110}-(1×2): a First-Principles Molecular Dynamics Study. *Comput. Theor. Chem.* **2012**, *990*, 144–151.
- (99) Shen, X. J.; Lozano, A.; Dong, W.; Busnengo, H. F.; Yan, X. H. Towards Bond Selective Chemistry from First Principles: Methane on Metal Surfaces. *Phys. Rev. Lett.* **2014**, *112*, 046101.
- (100) Mastromatteo, M.; Jackson, B. The Dissociative Chemisorption of Methane on Ni(100) and Ni(111): Classical and Quantum Studies Base on the Reaction Path Hamiltonian. *J. Chem. Phys.* **2013**, *139*, 194701.
- (101) Garrett, B. C.; Truhlar, D. G. Wkb Approximation for the Reaction-Path Hamiltonian - Application to Variational Transition-State Theory, vibrationally Adiabatic Excited-State Barrier Heights, and Resonance Calculations. *J. Chem. Phys.* **1984**, *81*, 309–317.
- (102) Garrett, B. C.; Truhlar, D. G.; Bowman, J. M.; Wagner, A. F. Evaluation of Dynamic Approximations for Calculating the Effect of Vibrational-Excitation on Reaction-Rates - O + H₂(N=0,1) [-] OH(N=0,1) + H. *J. Phys. Chem.* **1986**, *90*, 4305–4311.
- (103) Yoon, S.; Holiday, R. J.; Sibert, E. L.; Crim, F. F. The Relative Reactivity of CH₃D Molecules with Excited Symmetric and Antisymmetric Stretching Vibrations. *J. Chem. Phys.* **2003**, *119*, 9568–9575.
- (104) Jiang, B.; Guo, H. Relative Efficacy of Vibrational Vs. Translational Excitation in Promoting Atom-Diatom Reactivity: Rigorous Examination of Polanyi's Rules and Proposition of Sudden Vector Projection (SVP) Model. *J. Chem. Phys.* **2013**, *138*, 234104.
- (105) Nattino, F.; Diaz, C.; Jackson, B.; Kroes, G. J. Effect of Surface Motion on the Rotational Quadrupole Alignment Parameter of D₂ Reacting on Cu(111). *Phys. Rev. Lett.* **2012**, *108*.
- (106) Mondal, A.; Wijzenbroek, M.; Bonfanti, M.; Diaz, C.; Kroes, G. J. Thermal Lattice Expansion Effect on Reactive Scattering of H₂ from Cu(111) at T_s=925 K. *J. Phys. Chem. A* **2013**, *117*, 8770–8781.
- (107) Bonfanti, M.; Diaz, C.; Somers, M. F.; Kroes, G. J. Hydrogen dissociation on Cu(111): the influence of lattice motion. Part I. *Phys. Chem. Chem. Phys.* **2011**, *13*, 4552–4561.
- (108) Seenivasan, H.; Tiwari, A. K. Water Dissociation on Ni(100) and Ni(111): Effect of Surface Temperature on Reactivity. *J. Chem. Phys.* **2013**, *139*.
- (109) Hundt, P. M.; Jiang, B.; van Reijzen, M. E.; Guo, H.; Beck, R. D. vibrationally Promoted Dissociation of Water on Ni(111). *Science* **2014**, *344*, 504–507.
- (110) Jiang, B.; Li, J.; Xie, D. Q.; Guo, H. Effects of Reactant Internal Excitation and Orientation on Dissociative Chemisorption of H₂O on Cu(111): Quasi-Seven-Dimensional Quantum Dynamics on a Refined Potential Energy Surface. *J. Chem. Phys.* **2013**, *138*, 044704.

- (111) Jiang, B.; Ren, X. F.; Xie, D. Q.; Guo, H. Enhancing Dissociative Chemisorption of H₂O on Cu(111) via Vibrational Excitation. *Proc. Natl. Acad. Sci.* **2012**, *109*, 10224–10227.
- (112) Jiang, B.; Xie, D.; Guo, H. vibrationally Mediated Bond Selective Dissociative Chemisorption of HOD on Cu(111). *Chem. Sci.* **2013**, *4*, 503–508.
- (113) Killelea, D. R.; Utz, A. L. On the Origin of Mode- And Bond-Selectivity in vibrationally Mediated Reactions on Surfaces. *Phys. Chem. Chem. Phys.* **2013**, *15*, 20545–20554.